AIMS Mathematics, 10(11): 25380–25405.
DOI:10.3934/math.20251124
Received: 10 August 2025
Revised: 21 October 2025
Accepted: 22 October 2025
Published: 05 November 2025

https://www.aimspress.com/journal/Math

Research article

Hopf bifurcation and hybrid control in a delayed predator-prey model

Jiao-Guo Wang[1,2] **and Xin-You Meng**[1,3,*]

[1] School of Automation and Electrical Engineering, Lanzhou University of Technology, Lanzhou, Gansu 730050, China

[2] College of General Education, Lanzhou University of Information Science and Technology, Lanzhou, Gansu 730300, China

[3] School of Science, Lanzhou University of Technology, Lanzhou, Gansu 730050, China

* **Correspondence:** Email: xymeng@lut.edu.cn.

Abstract: In this paper, we considered a predator-prey model with self-feedback delay to investigate its Hopf bifurcation and control. First, non-negativity, boundedness, and the existence and uniqueness of solutions were discussed. Next, the conditions of the existence of the unique positive equilibrium were analyzed. Then, by using delay as the bifurcation parameter, the local stability of the positive equilibrium, and the existence and characteristics of Hopf bifurcation were investigated. Furthermore, by designing a hybrid controller integrating linear time-delayed state feedback and parametric regulation, the local asymptotic stability at the positive equilibrium was achieved within the target delay interval. Finally, numerical simulations verified the theoretical results. From the perspectives of unknown and known control gains, the stability switching mechanism and the maximum stable delay interval were explored. The results demonstrated that the proposed hybrid controller maintains system stability over a wider delay range and eliminates population extinction risks, providing a theoretical basis for stability regulation in ecosystem management.

Keywords: predator-prey; delay; Hopf bifurcation; hybrid control
Mathematics Subject Classification: 34H20, 34K18, 37G15, 92B05

1. Introduction

In natural ecosystems, the interactions between predator and prey are highly complex. To investigate their dynamic behaviors, Lotka and Volterra proposed the classic Lotka-Volterra model [1, 2], which laid a crucial foundation for subsequent research. Inspired by this model, numerous researchers have extended its framework by taking in more factors, such as selecting functional response functions, incorporating non-lethal effects, and introducing growth delay effects, to simulate complex ecological

interactions among multiple species [3]. To enhance model realism, some scholars have focused on key biological factors. For example, fear effects significantly suppress juvenile reproduction and adult survival [4, 5]. Refuge effects lead to sustained increases in prey density and drive Turing pattern evolution [6]. Harvesting of economically valuable species serves a dual role in sustaining human subsistence and maintaining ecological balance [7]. Integrating these external factors to reflect real-world conditions has propelled significant advancements in this field [8–10].

Wang et al. [8] investigated the impact of the fear effect in a Beddington-DeAngelis prey-predator model with prey refuge as follows:

$$\begin{cases} \dfrac{\mathrm{d}x}{\mathrm{d}t} = rx(\dfrac{1}{1+Ky} - \dfrac{x}{k}) - \dfrac{\beta(1-m)xy}{\alpha_1 + (1-m)x + y} - q_1 A x, \\ \dfrac{\mathrm{d}y}{\mathrm{d}t} = \dfrac{\beta_1(1-m)xy}{\alpha_1 + (1-m)x + y} - \theta_1 y - \dfrac{q_2 B y}{p_1 q_2 B + p_2 y}, \end{cases} \tag{1.1}$$

where $x(t)$ and $y(t)$ denote the densities of prey and predator populations at time t, respectively. $K > 0$ refers to the level of fear and $m \in [0, 1)$ is the rate of refuge of prey. Other parameters' biological interpretations are detailed in [8]. The authors conducted an in-depth analysis of the impact of fear and refuge effects on this model, and systematically investigated codimension-one and codimension-two bifurcations.

Delays are prevalent in ecological, neural, and physiological systems, manifesting as maturation periods in population reproduction, signal transmission lags, or resource regeneration intervals [11]. Studies demonstrate that exceeding critical delay thresholds destabilizes steady states, inducing complex dynamics such as chaotic oscillations, periodic solutions, or multistability [12–14]. Ignoring inherent population delays causes model distortion, while delay-induced Hopf bifurcation serves as the core mechanism for the transition from steady states to periodic oscillations, holding significant theoretical value in biomathematics [15]. In population ecology, delays can trigger Hopf bifurcation by modulating interspecific or intraspecific feedback. Xue et al. [16] investigated the impact of non-local delay on vegetation pattern dynamics and discovered that delay intensity significantly boosts vegetation biomass. Zhu et al. [17] studied the regulatory effect of intraspecific delay on the Michaelis-Menten-type harvesting Lotka-Volterra mutualistic model.

As a result, delay has become the theoretical foundation for analyzing oscillations, bursts, and spatial patterns in biological systems by inducing Hopf bifurcations. Based on the aforementioned viewpoints, and assuming that prey density is affected by delay effect caused by competition for environmental resources, then we can modify model (1.1) as follows:

$$\begin{cases} \dfrac{\mathrm{d}x}{\mathrm{d}t} = rx(\dfrac{1}{1+Ky} - \dfrac{x(t-\tau)}{k}) - \dfrac{\beta(1-m)xy}{\alpha_1 + (1-m)x + y} - q_1 A x, \\ \dfrac{\mathrm{d}y}{\mathrm{d}t} = \dfrac{\beta_1(1-m)xy}{\alpha_1 + (1-m)x + y} - \theta_1 y - \dfrac{q_2 B y}{p_1 q_2 B + p_2 y}, \end{cases} \tag{1.2}$$

where τ is a self-feedback delay induced by prey competition for resources. All other parameters are positive real numbers. Before starting the detailed study, we denote $\alpha = \frac{r}{k}$, $E_1 = q_1 A$, $E_2 = q_2 B$, and

model (1.2) is as follows:

$$\begin{cases} \dfrac{\mathrm{d}x}{\mathrm{d}t} = x\left(\dfrac{r}{1+Ky} - \alpha x(t-\tau)\right) - \dfrac{\beta(1-m)xy}{\alpha_1 + (1-m)x + y} - E_1 x, \\ \dfrac{\mathrm{d}y}{\mathrm{d}t} = \dfrac{\beta_1(1-m)xy}{\alpha_1 + (1-m)x + y} - \theta_1 y - \dfrac{E_2 y}{p_1 E_2 + p_2 y}. \end{cases} \tag{1.3}$$

The initial conditions of model (1.3) are

$$x(\theta) = \phi_1(\theta),\ y(\theta) = \phi_2(\theta),\ \theta \in [-\tau, 0),\ \phi_1(0) > 0,\ \phi_2(0) > 0.$$

Indeed, bifurcations observed in engineering fields such as bridge construction, aerospace, machinery, and power systems are closely related to chaos. When parameters cross their critical thresholds, the occurrence of bifurcation induces destructive dynamic responses including jumps, hysteresis, oscillatory instability, and even sudden collapse. The algal bloom phenomenon can be substantiated by bifurcation/chaotic behaviors induced by parameter variations [18], whereas the fishery collapse mechanism has been validated through dynamical features including transcritical bifurcation, saddle-node bifurcation, and Hopf bifurcation in a delay-induced predator-prey model [19].

To suppress adverse ecological phenomena induced by bifurcations and enhance system stability, researchers are focusing on bifurcation control through biomass feedback. This approach, which involves designing controllers to alter the bifurcation characteristics of nonlinear systems for eliminating harmful dynamic behaviors and inducing desired ones, is rapidly emerging as a frontier direction in the field of nonlinear dynamics [20]. After May's pioneering work in the 20th century [21], extensive developments have been used in ecology, biology, and applied engineering. Researchers have used the state feedback control method [22–24], parameter perturbations [25–27], hybrid control (combining feedback and parameter perturbations) [28–30], and time-delayed state feedback control [31–33] to effectively suppress bifurcations. Zhang et al. [23] considered the Willametto-Rössler system, proposed a state feedback control method, and investigated the anti-control of Hopf bifurcation in this system. Mu et al. [30] investigated hybrid control of Hopf bifurcation in a spatial prey-predator model with cooperative hunting and fear effect. Ou et al. [33] established a delay control framework for bifurcation regulation and stability enhancement in delayed predator-prey system, contributing to ecological balance maintenance. Although biological control is an effective means of intervening in ecosystems, research on the application of hybrid control that combines time-delayed state feedback and parameter regulation in predator-prey systems remains insufficient.

The main contributions of this study are summarized as follows: we introduce a self-feedback delay induced by prey competition for resources and discuss the critical conditions about Hopf bifurcation. Based on the above results, we propose an innovative hybrid control strategy that effectively regulates the stability region of model (1.3) and the onset time of Hopf bifurcation. Furthermore, numerical analysis demonstrates that gain conditions ensuring system stability under arbitrary delay can be derived when control gains are unknown, providing theoretical guidance for gain selection , and that the maximum stable delay interval can be quantified when gains are specified, thereby laying the foundation for enhancing system performance through delay regulation.

The remaining of this paper is organized as follows: in Section 2, the peculiarities of the solutions (e.g., non-negativeness, boundedness, existence, and uniqueness) of model (1.3) are

discussed. In Section 3, the existence of the positive equilibrium is demonstrated. In Section 4, the local stability of the positive equilibrium and the existence of Hopf bifurcation of model (1.3) are investigated. Based on normal form theory and center manifold theorem, directions of Hopf bifurcation and stability of the bifurcating periodic solutions are also discussed. In Section 5, the local stability of the positive equilibrium and the existence of Hopf bifurcation of model (1.3) with hybrid control strategy are analyzed. In Section 6, numerical simulations are given to illustrate the results. Finally, conclusions and brief discussions are presented in the last section.

2. Well-posedness

In this part, we will discuss the well-posedness of solutions of model (1.3) by using fixed point theory, inequality techniques, and construction of a reasonable function. Biologically, this is important due to population feasibility and finiteness. Thus, we study the dynamics of model (1.3) within the first quadrant ($\mathbb{R}^2_+$).

Theorem 2.1. *All solutions of model (1.3) starting with $\mathbb{R}^2_+$ are non-negative.*

Proof. From the first equation of model (1.3), we obtain that

$$x(t) = x(0)\exp\Big[\int_0^t \left(\frac{r}{1+Ky(\varsigma)} - \alpha x(\varsigma-\tau) - \frac{\beta(1-m)y(\varsigma)}{\alpha_1+(1-m)x(\varsigma)+y(\varsigma)} - E_1\right) d\varsigma\Big].$$

From the second equation of model (1.3), we have

$$y(t) = y(0)\exp\Big[\int_0^t \left(\frac{\beta_1(1-m)x(\varsigma)}{\alpha_1+(1-m)x(\varsigma)+y(\varsigma)} - \theta_1 - \frac{E_2}{p_1E_2+p_2y(\varsigma)}\right) d\varsigma\Big].$$

This implies that $x(t) > 0$, $y(t) > 0$ whenever $x(0) > 0,\ y(0) > 0$. □

Theorem 2.2. *If $\beta_1 - \beta - \theta_1 + E_1 < 0$ holds, then all solutions of model (1.3) starting with $\mathbb{R}^2_+$ are uniformly bounded.*

Proof. Assuming that $\varpi(t) = x(t) + y(t)$, then

$$\begin{aligned}
\frac{\mathrm{d}\varpi(t)}{\mathrm{d}t} &= \frac{\mathrm{d}x(t)}{\mathrm{d}t} + \frac{\mathrm{d}y(t)}{\mathrm{d}t} \\
&= \frac{rx}{1+Ky} - \alpha x x(t-\tau) - E_1x + \frac{(\beta_1-\beta)(1-m)xy}{\alpha_1+(1-m)x+y} - \theta_1 y - \frac{E_2y}{p_1E_2+p_2y} \\
&\le (r-E_1)x - \alpha x^2 + \frac{(\beta_1-\beta)(1-m)xy}{\alpha_1+(1-m)x+y} - \theta_1 y \\
&\le -E_1(x+y) + rx - \alpha x^2 + (\beta_1-\beta-\theta_1+E_1)y.
\end{aligned}$$

If $\beta_1 - \beta - \theta_1 + E_1 < 0$ holds, then

$$\frac{\mathrm{d}\varpi(t)}{\mathrm{d}t} = -E_1\varpi(t) + l,$$

where $l = \max(rx - \alpha x^2) = \frac{r^2}{4\alpha}$. Therefore, by using the theorem of differential inequality [34], we have

$$0 \le \varpi(t) \le \varpi(0)e^{-E_1t} + \frac{l}{E_1} - \frac{l}{E_1}e^{-E_1t}.$$

Since $E_1 > 0$, then $0 \leq \varpi(t) \leq \frac{l}{E_1}$, $t \to \infty$. Therefore, all solutions of model (1.3) are uniformly bounded. □

Theorem 2.3. *Denote* $\Phi = \{x, y \in \mathbb{R}^2_+ : max\{|x|, |y|\} \leq \mathcal{M}\}$, *where* $\mathcal{M} = \frac{r^2}{4\alpha E_1}$. *Under the condition* $\beta_1 - \beta - \theta_1 + E_1 < 0$, *for each* $(x(0), y(0)) \in \Phi$, *model (1.3) has a unique solution* $U = (x, y) \in \Phi$.

Proof. Define

$$F(U) = [F_1(U), F_2(U)],$$

where $U = (x, y)$, and

$$F_1(U) = \frac{rx}{1+Ky} - \alpha x x(t-\tau) - \frac{\beta(1-m)xy}{\alpha_1+(1-m)x+y} - E_1 x,\ F_2(U) = \frac{\beta_1(1-m)xy}{\alpha_1+(1-m)x+y} - \theta_1 y - \frac{E_2 y}{p_1E_2+p_2y}.$$

For every $U, \bar{U} \in \Phi$, we have

$$\begin{aligned}
\| F(U) - F(\bar{U}) \| &= \Big|(\frac{rx}{1+Ky} - \frac{r\bar{x}}{1+K\bar{y}}) - \alpha(xx(t-\tau) - \bar{x}\bar{x}(t-\tau)) - E_1(x-\bar{x}) \\
&- \beta(1-m)\Big(\frac{xy}{\alpha_1+(1-m)x+y} - \frac{\bar{x}\bar{y}}{\alpha_1+(1-m)\bar{x}+\bar{y}}\Big)\Big| \\
&+ \Big|\beta_1(1-m)\Big(\frac{xy}{\alpha_1+(1-m)x+y} - \frac{\bar{x}\bar{y}}{\alpha_1+(1-m)\bar{x}+\bar{y}}\Big) - \theta_1(x-\bar{x}) \\
&- E_2\Big(\frac{y}{p_1E_2+p_2y} - \frac{\bar{y}}{p_1E_2+p_2\bar{y}}\Big)\Big| \\
&\leq (r + 2\alpha\mathcal{M} + E_1)|x-\bar{x}| + (\frac{1}{p} + \theta_1)|y-\bar{y}| + \frac{(\beta+\beta_1)(1-m)}{\alpha_1}|xy - \bar{x}\bar{y}| \\
&= (r + 2\alpha\mathcal{M} + E_1)|x-\bar{x}| + (\frac{1}{p} + \theta_1)|y-\bar{y}| \\
&+ \frac{(\beta+\beta_1)(1-m)}{\alpha_1}|xy - \bar{x}y + \bar{x}y - \bar{x}\bar{y}| \\
&\leq \rho_1|x-\bar{x}| + \rho_2|y-\bar{y}| \\
&\leq \rho \| U - \bar{U} \|,
\end{aligned}$$

where $\rho_1 = (r + 2\alpha\mathcal{M} + E_1 + \frac{(\beta+\beta_1)(1-m)\mathcal{M}}{\alpha_1})$, $\rho_2 = (\frac{1}{p} + \theta_1 + \frac{(\beta+\beta_1)(1-m)\mathcal{M}}{\alpha_1})$, and $\rho = \max\{\rho_1, \rho_2\}$. Thus, $F(U)$ obeys the Lipschitz condition for U. Using the fixed point theorem [35], the above conclusion is right. □

3. Existence of a unique positive equilibrium

This section will prove that model (1.3) has a unique positive equilibrium under specific parameter conditions. We assume that $C^*(x^*, y^*)$ is the positive equilibrium of model (1.3), and define

$$\begin{cases} F_1(x,y) = \frac{r}{1+Ky} - \alpha x - \frac{\beta(1-m)y}{\alpha_1+(1-m)x+y} - E_1, \\ F_2(x,y) = \frac{\beta_1(1-m)x}{\alpha_1+(1-m)x+y} - \theta_1 - \frac{E_2}{p_1E_2+p_2y}. \end{cases} \tag{3.1}$$

Then the positive equilibrium $C^*(x^*, y^*)$ of model (1.3) satisfies $F_1(x, y) = 0$ and $F_2(x, y) = 0$. Moreover, if $\frac{\partial F_1(x,y)}{\partial y}\Big|_{(x^*,y^*)} \neq 0$, $\frac{\partial F_2(x,y)}{\partial y}\Big|_{(x^*,y^*)} \neq 0$, according to the implicit function theorem, then

functions $y = f_1(x)$ and $y = f_2(x)$ can be defined by equations $F_1(x, y) = 0$ and $F_2(x, y) = 0$, respectively. Furthermore, we assume that functions $y = f_1(x)$ and $y = f_2(x)$ are different monotonic (one strictly increasing and the other strictly decreasing) in the first quadrant. If the above functions intersect in the first quadrant, then the intersection point is unique.

For the first equation of Eq (3.1), when $y = 0$, we have $x = \frac{r-E_1}{\alpha} =: x_1 > 0$ if the condition $(H_1) : r - E_1 > 0$ holds. When $x = 0$, we have

$$\eta_1 y^2 + \eta_2 y + \eta_3 = 0, \tag{3.2}$$

where $\eta_1 = KE_1 + K\beta(1 - m) > 0$, $\eta_2 = \beta(1 - m) + \alpha_1 E_1 K + E_1 - r$, $\eta_3 = \alpha_1(E_1 - r)$.

It should be noted that $\eta_3 < 0$ under the condition (H_1). Therefore, $\Delta = \eta_2^2 - 4\eta_1\eta_3 > 0$, then Eq (3.2) has a unique positive real root $y = \frac{\sqrt{\Delta}-\eta_2}{2\eta_1} =: y_1 \in (0, +\infty)$. Taking the partial derivatives of $F_1(x, y)$ with respect to x and y for the first equation of Eq (3.1), we get

$$\frac{\partial F_1(x,y)}{\partial x} = \frac{\beta(1-m)^2 y}{[\alpha_1 + (1-m)x + y]^2} - \alpha, \ \frac{\partial F_1(x,y)}{\partial y} = -\frac{Kr}{(1+Ky)^2} - \frac{\beta(1-m)[\alpha_1 + (1-m)x]}{[\alpha_1 + (1-m)x + y]^2}.$$

Clearly, $\frac{\partial F_1(x,y)}{\partial y} < 0$. If the condition $(H_2) : 4E_1\alpha^2 > \beta r^2(1 - m)^2$ holds, then $\frac{\mathrm{d}y}{\mathrm{d}x} < 0$. Thus, $y = f_1(x)$ passes through the points $(x_1, 0)$ and $(0, y_1)$, where $x_1 > 0$ and $y_1 > 0$ under the condition (H_1). Furthermore, $y = f_1(x)$ is a decreasing function under the condition (H_2).

For the second equation of Eq (3.1), when $y = 0$, we have $x = \frac{\alpha_1(\theta_1 + \frac{E_2}{p_1})}{(\beta - \theta_1 - \frac{1}{p_1})(1-m)} =: x_2 > 0$ if the condition $(H_3) : \beta - \theta_1 - \frac{1}{p_1} > 0$ holds. When $x = 0$, we have $y = -\frac{\theta_1 p_1 E_2 + E_2}{\theta_1 p_2} =: y_2 < 0$. Taking the partial derivatives of $F_2(x, y)$ with respect to x and y for the second equation of Eq (3.1), we get

$$\frac{\partial F_2(x,y)}{\partial x} = \frac{\beta(1-m)(\alpha_1 + y)}{[\alpha_1 + (1-m)x + y]^2}, \ \frac{\partial F_2(x,y)}{\partial y} = \frac{p_2}{(p_1 E_2 + p_2 y)^2} - \frac{\beta_1(1-m)x}{[\alpha_1 + (1-m)x + y]^2}.$$

Clearly, $\frac{\partial F_2(x,y)}{\partial x} > 0$. If the condition $(H_4) : \theta_1 > \frac{\beta_1(1-m)r^2}{4\alpha\alpha_1 E_1 + (1-m)r^2} - \frac{16p_1\alpha^2 E_1^2 E_2^2}{(4p_1\alpha E_1 E_2 + p_2 r^2)^2}$ holds, then $\frac{\mathrm{d}y}{\mathrm{d}x} < 0$. $y = f_2(x)$ passes through the points $(x_2, 0)$ and $(0, y_2)$, where $x_2 > 0$ and $y_2 < 0$ under the condition (H_3). Thus, $y = f_2(x)$ is an increasing function under the condition (H_4).

If $(H_5) : x_2 < x_1$ holds, then $y = f_1(x)$ and $y = f_2(x)$ have a unique intersection in the first quadrant, which means that Eq (3.1) has a unique positive equilibrium $C^*(x^*, y^*)$. Thus, we have the following theorem.

Theorem 3.1. *The model (1.3) has a unique positive equilibrium $C^*(x^*, y^*)$ if conditions (H_1)–(H_5) hold.*

Remark 1. *The existence of multiple positive equilibria has been investigated in [8], but we give a unique positive equilibrium by using the other method that is not used in that work [8]. The local asymptotic stability of non-negative equilibria has been analyzed in [8]. Therefore, we do not discuss it again, and only discuss the bifurcation of a unique positive equilibrium.*

4. Bifurcation

4.1. Hopf bifurcation

In this part, we will only investigate the effect of delay on the dynamics of model (1.3) around the positive equilibrium $C^*(x^*, y^*)$. For convenience, we first translate the positive equilibrium $C^*(x^*, y^*)$

to the origin by setting $\overline{x} = x - x^*$ and $\overline{y} = y - y^*$, and drop the bar for convenience of notation. Then, the linearized system of model (1.3) can be obtained

$$\begin{cases} \dfrac{\mathrm{d}x}{\mathrm{d}t} = a_{11}x + a_{12}y + b_{11}x(t-\tau), \\ \dfrac{\mathrm{d}y}{\mathrm{d}t} = a_{21}x + a_{22}y, \end{cases} \tag{4.1}$$

where

$$a_{11} = \frac{r}{1+Ky^*} - \alpha x^* - \frac{\beta(1-m)y^*(\alpha_1+y^*)}{[\alpha_1+(1-m)x^*+y^*]^2} - E_1,\ a_{12} = -\frac{rKx^*}{(1+Ky^*)^2} - \frac{\beta(1-m)x^*[\alpha_1+(1-m)x^*]}{[\alpha_1+(1-m)x^*+y^*]^2},$$

$$b_{11} = -\alpha x^*,\ a_{21} = \frac{\beta_1(1-m)y^*(\alpha_1+y^*)}{[\alpha_1+(1-m)x^*+y^*]^2},\ a_{22} = \frac{\beta_1(1-m)x^*[\alpha_1+(1-m)x^*]}{[\alpha_1+(1-m)x^*+y^*]^2} - \theta_1 - \frac{p_1E_2^2}{(p_1E_2+p_2y^*)^2}.$$

The characteristic equation of model (4.1) around $C^*(x^*, y^*)$ takes the following form

$$\lambda^2 - (a_{11}+a_{22})\lambda - b_{11}(\lambda - a_{22})e^{-\lambda\tau} + a_{11}a_{22} - a_{12}a_{21} = 0. \tag{4.2}$$

Assuming that

$$(H_6) : a_{11} + a_{22} + b_{11} < 0,\ (a_{11}+b_{11})a_{22} - a_{12}a_{21} > 0.$$

It is easy to know that model (1.3) without delay is locally asymptotically stable at the positive equilibrium $C^*(x^*, y^*)$ if the condition (H_6) holds.

Next, subsequent analysis will systematically elucidate the mechanisms through which delay influences the stability of state in model (1.3). Suppose that Eq (4.2) admits a root $i\omega$ ($\omega \geq 0$), then it follows

$$-\omega^2 - (a_{11}+a_{22})i\omega - b_{11}(i\omega - a_{22})e^{-i\omega\tau} + a_{11}a_{22} - a_{12}a_{21} = 0. \tag{4.3}$$

By Eq (4.3), we have

$$\begin{cases} -b_{11}\omega\sin(\omega\tau) + a_{22}b_{11}\cos(\omega\tau) = \omega^2 - a_{11}a_{22} + a_{12}a_{21}, \\ -b_{11}\omega\cos(\omega\tau) - a_{22}b_{11}\sin(\omega\tau) = (a_{11}+a_{22})\omega. \end{cases} \tag{4.4}$$

Additionally, Eq (4.4) demonstrates that

$$G_1(Z) := Z^2 + PZ + Q = 0, \tag{4.5}$$

where $Z = \omega^2$, $P = a_{11}^2 + a_{22}^2 + 2a_{12}a_{21} - b_{11}^2$ and $Q = (a_{12}a_{21} - a_{11}a_{22})^2 - a_{22}^2b_{11}^2$. After the discussion about the roots of Eq (4.5), we can get three conditions as follows:

$$(H_7) : P > 0 \text{ and } Q > 0,\ (H_8) : Q < 0,\ (H_9) : P^2 > 4Q, P < 0 \text{ and } Q > 0.$$

If the condition (H_7) is true, then Eq (4.5) has no positive root, which means that such ω does not exist. Thus, $C^*(x^*, y^*)$ is locally asymptotically stable for all $\tau > 0$ if conditions (H_6) and (H_7) hold. Moreover, if (H_6) fails and (H_7) holds, then $C^*(x^*, y^*)$ is unstable for all $\tau > 0$.

If the condition (H_8) is true, then there exists a unique positive root ω_0^2 for Eq (4.5). Substituting ω_0 into Eq (4.4), it follows that

$$\tau_j = \frac{1}{\omega_0}\left[\arccos S_1 + 2j\pi\right],$$

where $j = 0, 1, 2\cdots$, and $S_1 = \frac{-a_{11}\omega_0^2 - a_{11}a_{22}^2 + a_{22}a_{12}a_{21}}{b_{11}(a_{22}^2+\omega_0^2)}$.

If condition (H_9) is true, Eq (4.5) has positive roots ω_+^2 and ω_-^2. Substituting $\omega_\pm$ into Eq (4.4), it follows that

$$\tau_j^\pm = \frac{1}{\omega_\pm}\left[\arccos S_2 + 2j\pi\right],$$

where $j = 0, 1, 2\cdots$, $S_2 = \frac{-a_{11}\omega_\pm^2 - a_{11}a_{22}^2 + a_{22}a_{12}a_{21}}{b_{11}(a_{22}^2+\omega_\pm^2)}$.

Let $\lambda(\tau_j) = i\omega_0$ be a root of Eq (4.2). Differentiating both sides of Eq (4.2) with respect to τ, we get

$$\left(\frac{\mathrm{d}\lambda}{\mathrm{d}\tau}\right)^{-1} = \frac{2\lambda - (a_{11}+a_{22}) - b_{11}e^{-\lambda\tau}}{-b_{11}\lambda(\lambda - a_{22})e^{-\lambda\tau}} - \frac{\tau}{\lambda}.$$

By a series of computations, we further get

$$\mathrm{Re}\left(\frac{\mathrm{d}\lambda}{\mathrm{d}\tau}\right)^{-1}\Big|_{\tau=\tau_j,\lambda=i\omega_0} = \frac{G_1'(\omega_0^2)}{b_{11}^2(a_{22}^2+\omega_0^2)}.$$

When (H_8) holds, since $G_1(0) = Q < 0$, $G_1(\infty) = \infty$, we obtain $G_1'(\omega_0^2) > 0$. It is well known that

$$\mathrm{sign}\left\{\mathrm{Re}\left(\frac{\mathrm{d}\lambda}{\mathrm{d}\tau}\right)\right\}_{\tau=\tau_j,\lambda=i\omega_0} = \mathrm{sign}\left\{\mathrm{Re}\left(\frac{\mathrm{d}\lambda}{\mathrm{d}\tau}\right)^{-1}\right\}_{\tau=\tau_j,\lambda=i\omega_0} > 0.$$

In a similar way, let $\lambda(\tau_j^\pm) = i\omega_\pm$ be a root of Eq (4.2). When (H_9) holds, since $G_1(0) = Q > 0$, $G_1(\infty) = \infty$, we obtain $G_1'(\omega_-^2) < 0$ and $G_1'(\omega_+^2) > 0$. Therefore, we further get

$$\mathrm{sign}\left\{\mathrm{Re}\left(\frac{\mathrm{d}\lambda}{\mathrm{d}\tau}\right)\right\}_{\tau=\tau_j^-,\lambda=i\omega_-} < 0,\ \mathrm{sign}\left\{\mathrm{Re}\left(\frac{\mathrm{d}\lambda}{\mathrm{d}\tau}\right)\right\}_{\tau=\tau_j^+,\lambda=i\omega_+} > 0.$$

As a consequence of the above analysis, we have the following results:

Theorem 4.1. *(i) If (H_6) and (H_7) hold, then the positive equilibrium $C^*(x^*, y^*)$ of model (1.3) is locally asymptotically stable when $\tau > 0$. If (H_6) fails but (H_7) holds, then $C^*(x^*, y^*)$ is unstable when $\tau > 0$.*
(ii) If (H_6) and (H_8) hold, then $C^*(x^*, y^*)$ is locally asymptotically stable when $\tau \in [0, \tau_0)$, but unstable when $\tau > \tau_0$. Moreover, when τ crosses the threshold value τ_0, model (1.3) loses its stability and Hopf bifurcation occurs at $C^*(x^*, y^*)$.
(iii) If (H_6) and (H_9) hold, then $C^*(x^*, y^*)$ is locally asymptotically stable for $\tau \in (0, \tau_0^+) \cup (\tau_0^-, \tau_1^+) \cup \cdots \cup (\tau_{j-1}^-, \tau_j^+) \cup \cdots$ and unstable for $\tau \in (\tau_0^+, \tau_0^-) \cup (\tau_1^+, \tau_1^-) \cup \cdots \cup (\tau_j^+, \tau_j^-) \cup \cdots$. In addition, the model (1.3) undergoes a Hopf bifurcation at $C^*(x^*, y^*)$ when $\tau = \tau_j^\pm$, $j = 0, 1, 2, \cdots$.

4.2. Properties of Hopf bifurcation

From Theorem 4.1, we have obtained the conditions for the existence of Hopf bifurcation when $\tau = \tau_0$. In this subsection, we will consider the direction of the Hopf bifurcation and the stability of bifurcating periodic solutions of model (1.3) by using the center manifold and normal form theories presented in [36].

Let $\tau = \tau_0 + \sigma$, $u_1(t) = x(\tau t) - x^*$, $u_2(t) = y(\tau t) - y^*$, and $u_t(\theta) = u(t+\theta)$ for $\theta \in [-1, 0]$. Model (1.3) becomes a functional differential equation in $\mathbb{C}([-1, 0], \mathbb{R}^2)$ as follows:

$$\dot{u}(t) = L_\sigma(u_t) + f(\sigma, u_t), \tag{4.6}$$

where $u(t) = (u_1(t), u_2(t))^T \in \mathbb{R}^2$, $L_\sigma : \mathbb{C} \to \mathbb{R}^2$, and $f : \mathbb{R} \times \mathbb{C} \to \mathbb{R}^2$ are defined by

$$L_\sigma(\phi) = (\tau_0 + \sigma)(J_1\phi(0) + J_2\phi(-1)),\ f(\sigma, \phi) = (f_1(\sigma, \phi), f_2(\sigma, \phi))^T,$$

where $\phi = (\phi_1(\theta), \phi_2(\theta)) \in \mathbb{C}[-1, 0], \mathbb{R}^2)$,

$$J_1 = \begin{pmatrix} a_{11} & a_{12} \\ a_{21} & a_{22} \end{pmatrix},\ J_2 = \begin{pmatrix} b_{11} & 0 \\ 0 & 0 \end{pmatrix},$$

and

$$f(\sigma, \phi) = (\tau_0 + \sigma) \begin{pmatrix} a_{120}\phi_1^2(0) + a_{111}\phi_1(0)\phi_2(0) + a_{102}\phi_2^2(0) - \alpha\phi_1(0)\phi_1(-1) \\ a_{220}\phi_1^2(0) + a_{211}\phi_1(0)\phi_2(0) + a_{202}\phi_2^2(0) \end{pmatrix}, \tag{4.7}$$

where

$$a_{120} = -\frac{\alpha}{2} + \frac{\beta(1-m)^2 y^*(\alpha_1+y^*)}{[\alpha_1+(1-m)x^*+y^*]^3},\ a_{111} = \frac{-rK}{(1+Ky^*)^2} - \frac{\beta(1-m)^2 x^*(\alpha_1+2y^*)+\alpha_1\beta(1-m)(\alpha_1+y^*)}{[\alpha_1+(1-m)x^*+y^*]^3},$$

$$a_{102} = \frac{\beta(1-m)x^*[\alpha_1+(1-m)x^*]}{[\alpha_1+(1-m)x^*+y^*]^3} + \frac{rK^2x^*}{(1+Ky^*)^3},\ a_{220} = -\frac{\beta_1(1-m)^2 y^*(\alpha_1+y^*)}{[\alpha_1+(1-m)x^*+y^*]^3},$$

$$a_{211} = \frac{\beta_1(1-m)^2 x^*(\alpha_1+2y^*)+\alpha_1\beta_1(1-m)(\alpha_1+y^*)}{[\alpha_1+(1-m)x^*+y^*]^3},\ a_{202} = -\frac{\beta_1(1-m)x^*[\alpha_1+(1-m)x^*]}{[\alpha_1+(1-m)x^*+y^*]^3} + \frac{p_1p_2E_2^2}{(p_1E_2+p_2y^*)^3}.$$

By the Riesz representation theorem [37], there exists a 2×2 matrix-valued function $\zeta(\theta, \sigma)$ of bounded variation for $\theta \in [-1, 0]$ such that

$$L_\sigma(\phi) = \int_{-1}^{0} \mathrm{d}\zeta(\theta, \sigma)\phi(\theta),\ \text{for } \phi \in \mathbb{C}([-1, 0], \mathbb{R}^2).$$

In fact, we can choose

$$\zeta(\theta, \sigma) = (\tau_0 + \sigma)[J_1\delta(\theta) - J_2\delta(\theta + 1)],$$

where $\delta(\theta)$ is a Dirac delta function.

For $\phi \in \mathbb{C}([-1, 0], \mathbb{R}^2)$, define

$$\mathrm{A}(\sigma)\phi(\theta) = \begin{cases} \dfrac{\mathrm{d}\phi(\theta)}{\mathrm{d}\theta}, & \theta \in [-1, 0), \\ \displaystyle\int_{-1}^{0} d\zeta(\theta, \sigma)\phi(\theta),\ \theta = 0, \end{cases}$$

and

$$\mathrm{R}(\sigma)\phi(\theta) = \begin{cases} 0, & \theta \in [-1, 0), \\ f(\sigma, \phi),\ \theta = 0. \end{cases}$$

Then model (4.6) can be rewritten as

$$\dot{u}_t = \mathrm{A}(\sigma)u_t + \mathrm{R}(\sigma)u_t. \tag{4.8}$$

For $\psi \in \mathbb{C}^1([-1, 0], \mathbb{R}^2)$, the adjoint operator A^* of A is defined as

$$\mathrm{A}^*\psi(s) = \begin{cases} -\dfrac{\mathrm{d}\psi(s)}{\mathrm{d}s}, & s \in (0, 1], \\ \displaystyle\int_{-1}^{0} \psi(-\xi)\mathrm{d}\zeta(\xi, 0),\ s = 0, \end{cases}$$

and a bilinear inner product

$$\langle \psi(s), \phi(\theta) \rangle = \bar{\psi}(0)\phi(0) - \int_{-1}^{0} \int_{\xi=0}^{\theta} \bar{\psi}(\xi - \theta) d\zeta(\theta) \phi(\xi) \mathrm{d}\xi, \tag{4.9}$$

where $\zeta(\theta) = \zeta(\theta, 0)$. From the above discussion, we can know that $\pm i\omega_0$ are the eigenvalues of A(0), thus $\pm i\omega_0$ are also the eigenvalues of A^*.

Let $q(\theta) = (1, \nu)^T e^{i\omega_0\tau_0\theta}$ be the eigenvector of A(0) corresponding to the eigenvalue $i\omega_0\tau_0$, and $q^*(s) = D(1, \nu^*)e^{-i\omega_0\tau_0 s}$ be the eigenvector of A^* corresponding to the eigenvalue $-i\omega_0\tau_0$. With the conditions $A(0)q(0) = i\omega_0 q(0)$, and $A^*q^*(0) = -i\omega_0 q^*(0)$, we obtain

$$[i\omega_0 I - (J_1 + J_2 e^{-i\omega_0\tau_0})]q(0) = 0, \;\; [-i\omega_0 I - (J_1^T + J_2^T e^{i\omega_0\tau_0})]q^*(0) = 0, \tag{4.10}$$

where I is an identity matrix of order 2. Solving Eq (4.10), we get $\nu = \frac{a_{21}}{i\omega_0 - a_{22}}$, $\nu^* = \frac{-a_{12}}{i\omega_0 + a_{22}}$.

By virtue of (4.9), it derives that

$$\begin{aligned}
\langle q^*, q \rangle &= \bar{q^*}(0)q(0) - \int_{-1}^{0} \int_{\xi=0}^{\theta} \bar{q}^*(\xi - \theta) \mathrm{d}\zeta(\theta) q(\xi) \mathrm{d}\xi \\
&= \bar{D}(1, \bar{\nu^*})(1, \nu)^T - \bar{D} \int_{\theta=-1}^{0} \int_{\xi=0}^{\theta} (1, \bar{\nu^*}) e^{-i\omega_0\tau_0(\xi-\theta)} \mathrm{d}\zeta(\theta)(1, \nu)^T e^{i\omega_0\tau_0\xi} \mathrm{d}\xi \\
&= \bar{D}(1 + \nu\bar{\nu^*} + \tau_0 b_{11} e^{-i\omega_0\tau_0}).
\end{aligned}$$

In order to satisfy that $\langle q^*, q \rangle = 1$ and $\langle q^*, \bar{q} \rangle = 0$, we can choose $\bar{D} = [1 + \nu\bar{\nu^*} + \tau_0 b_{11} e^{-i\omega_0\tau_0}]^{-1}$.

Next, we will compute the coordinates to detail the center manifold C_0 at $\sigma = 0$. Let μ_t be the solution of Eq (4.8) when $\sigma = 0$. Define

$$z(t) = \langle q^*, u_t \rangle, \;\; W(t, \theta) = u_t(\theta) - zq(\theta) - \bar{z}\bar{q(\theta)} = u_t(\theta) - 2\mathrm{Re}z(t)q(\theta). \tag{4.11}$$

On the center manifold C_0, it derives that

$$W(t, \theta) = W(z(t), \bar{z}(t), \theta) = W_{20}(\theta)\frac{z^2}{2} + W_{11}(\theta)z\bar{z} + W_{02}(\theta)\frac{\bar{z}^2}{2} + \cdots, \tag{4.12}$$

where z and $\bar{z}$ are local coordinates for C_0 in the direction of q^* and $\bar{q}^*$, respectively. When u_t is real, W is also real. Therefore, we only consider real solutions. For the solution $u_t \in C_0$ of Eq (4.8), since $\sigma = 0$, then we have

$$\dot{z}(t) = \langle q^*, \dot{u}(t) \rangle = \langle q^*, \mathrm{A}(0)u_t + \mathrm{R}(0)u_t \rangle = \langle A^*(0)q^*, u_t \rangle + \bar{q}^*(0)f(0, u_t) = i\omega_0\tau_0 z(t) + g(z, \bar{z}),$$

where

$$g(z, \bar{z}) = \bar{q}^*(0)f(0)(W(z, \bar{z}, 0) + 2\mathrm{Re}(z(t)q(\theta))) = g_{20}\frac{z^2}{2} + g_{11}z\bar{z} + g_{02}\frac{\bar{z}^2}{2} + g_{21}\frac{z^2\bar{z}}{2} + \cdots. \tag{4.13}$$

It follows from (4.11) and (4.12) that

$$u_t(\theta) = W_{20}(\theta)\tfrac{z^2}{2} + W_{11}(\theta)z\bar{z} + W_{02}(\theta)\tfrac{\bar{z}^2}{2} + (1, \nu)^T e^{i\omega_0\tau_0\theta} z + (1, \bar{\nu^*})^T e^{-i\omega_0\tau_0\theta}\bar{z} + \cdots.$$

From (4.7) and (4.13), it derives that

$$\begin{aligned} g(z,\bar{z}) = &\left[2\tau_0\bar{D}(k_{11}+k_{21}\bar{\nu}*)\right]\frac{z^2}{2} + \left[\tau_0\bar{D}(k_{12}+k_{22}\bar{\nu}*)\right]z\bar{z} \\ &+ \left[2\tau_0\bar{D}(k_{13}+k_{23}\bar{\nu}*)\right]\frac{z^2}{2} + \left[\tau_0\bar{D}(k_{14}+k_{24}\bar{\nu}*)\right]\frac{z^2\bar{z}}{2} + \cdots, \end{aligned} \tag{4.14}$$

where

$$\begin{aligned} &k_{11} = a_{120} + a_{111}\nu - \alpha e^{i\omega_0\tau_0},\ k_{21} = a_{220} + a_{211}\nu,\ k_{12} = 2a_{120} + a_{111}\nu - \alpha(e^{-i\omega_0\tau_0} + e^{i\omega_0\tau_0}), \\ &k_{22} = 2a_{220} + a_{111} + a_{211}\nu + 2a_{102}\nu,\ k_{13} = a_{120} - \alpha e^{i\omega_0\tau_0},\ k_{23} = a_{220} + a_{111}, \\ &k_{14} = 2a_{120}\left[W_{20}^{(1)}(0) + 2W_{11}^{(1)}(0)\right] + a_{111}\left[2\nu W_{11}^{(1)}(0) + 2W_{11}^{(2)}(0) + W_{20}^{(2)}(0)\right] \\ &\quad + 4a_{102}\nu W_{11}^{(1)}(0) - \alpha\left[e^{i\omega_0\tau_0}W_{20}^{(1)}(0) + 2e^{-i\omega_0\tau_0}W_{11}^{(1)}(0) + 2W_{11}^{(1)}(-1) + W_{20}^{(1)}(-1)\right], \\ &k_{24} = a_{111}W_{20}^{(1)}(0) + 2a_{220}\left[W_{20}^{(1)}(0) + 2W_{11}^{(1)}(0)\right] + a_{211}\left[2\nu W_{11}^{(1)}(0) + 2W_{11}^{(2)}(0) + W_{20}^{(2)}(0)\right] \\ &\quad + 2a_{102}\nu W_{20}^{(2)}(0) + 4\nu a_{202}W_{11}^{(1)}(0). \end{aligned}$$

By comparing coefficients with (4.13) and (4.14), it derives that

$$\begin{aligned} &g_{20} = 2\tau_0\bar{D}(k_{11}+k_{21}\bar{\nu}*),\ g_{11} = \tau_0\bar{D}(k_{12}+k_{22}\bar{\nu}*), \\ &g_{02} = 2\tau_0\bar{D}(k_{13}+k_{23}\bar{\nu}*),\ g_{21} = \tau_0\bar{D}(k_{14}+k_{24}\bar{\nu}*). \end{aligned}$$

Since W_{11} and W_{20} are still unknown, we still compute them. By virtue of (4.8) and (4.11), we have

$$\begin{aligned} \dot{W} &= \dot{u}_t - \dot{z}q - \dot{\bar{z}}\bar{q} \\ &= \begin{cases} A(0)W - 2\,\mathrm{Re}\left\{\bar{q}^*(0)f_0q(\theta)\right\}, & \theta \in [-1,0) \\ A(0)W - 2\,\mathrm{Re}\left\{\bar{q}^*(0)f_0q(0) + f_0(z,\bar{z})\right\}, & \theta = 0 \end{cases} \\ &\triangleq A(0)W + H(z,\bar{z},\theta), \end{aligned} \tag{4.15}$$

where

$$H(z,\bar{z},\theta) = H_{20}(\theta)\frac{z^2}{2} + H_{11}(\theta)z\bar{z} + H_{02}(\theta)\frac{\bar{z}^2}{2} + \cdots. \tag{4.16}$$

Substituting (4.16) into (4.15) and comparing coefficients, we can obtain

$$(A(0) - 2i\omega_0\tau_0)W_{20}(\theta) = -H_{20}(\theta),\ A(0)W_{11}(\theta) = -H_{11}(\theta). \tag{4.17}$$

From (4.15) and for $\theta \in [-1,0)$, we know that

$$H(z,\bar{z},\theta) = -q^*(0)f_0q(\theta) - q^*(0)\bar{f}_0\bar{q}(\theta) = -g(z,\bar{z})q(\theta) - \bar{g}(z,\bar{z})\bar{q}(\theta). \tag{4.18}$$

Using (4.13) in (4.18) and comparing coefficients with (4.16), it derives that

$$H_{20}(\theta) = -g_{20}q(\theta) - \bar{g}_{02}\bar{q}(\theta),\ H_{11}(\theta) = -g_{11}q(\theta) - \bar{g}_{11}\bar{q}(\theta). \tag{4.19}$$

Because $q(\theta) = (1,\nu)^T e^{i\omega_0\tau_0\theta}$, based on (4.17) and (4.19), we can obtain

$$\begin{aligned} W_{20}(\theta) &= \frac{ig_{20}q(0)}{\omega_0\tau_0}e^{i\omega_0\tau_0\theta} + \frac{i\bar{g}_{02}\bar{q}(0)}{3\omega_0\tau_0}e^{-i\omega_0\tau_0\theta} + M_1e^{2i\omega_0\tau_0\theta}, \\ W_{11}(\theta) &= \frac{-ig_{11}q(0)}{\omega_0\tau_0}e^{i\omega_0\theta} + \frac{i\bar{g}_{11}\bar{q}(0)}{\omega_0\tau_0}e^{-i\omega_0\tau_0\theta} + M_2, \end{aligned}$$

where $M_1 = (M_1^{(1)}, M_1^{(2)})^T$, $M_2 = (M_2^{(1)}, M_2^{(2)})^T$ are 2-dimensional constant vectors, and can be determined by setting $\theta = 0$ in $H(z, \bar{z}, \theta)$. Furthermore, we get

$$M_1 = 2 \begin{pmatrix} 2I\omega_0 - a_{11} - b_{11}e^{-2i\omega_0\tau_0} & -a_{12} \\ -a_{21} & 2i\omega_0 - a_{22} \end{pmatrix}^{-1} \begin{pmatrix} k_{11} \\ k_{21} \end{pmatrix},$$
$$M_2 = 2 \begin{pmatrix} 2I\omega_0 - a_{11} - b_{11} & -a_{12} \\ -a_{21} & -a_{22} \end{pmatrix}^{-1} \begin{pmatrix} k_{12} \\ k_{22} \end{pmatrix}.$$

Based on the above analysis, we can determine g_{21}, and the following quantities can be given

$$\begin{aligned} c_1(0) &= \frac{i}{2\omega_0\tau_0}\left(g_{20}g_{11} - 2|g_{11}|^2 - \frac{|g_{02}|^2}{3}\right) + \frac{g_{21}}{2}, \\ \mu_2 &= -\frac{\mathrm{Re}\{c_1(0)\}}{\mathrm{Re}\{\lambda'(\tau_0)\}}, \\ \beta_2 &= 2\mathrm{Re}\{c_1(0)\}, \\ T_2 &= -\frac{\mathrm{Im}\{c_1(0)\} + \mu_2\mathrm{Im}\{\lambda'(\tau_0)\}}{\omega_0\tau_0}. \end{aligned}$$

Thus, the properties of Hopf bifurcation at τ_0 are given by the following theorem:

Theorem 4.2. *(i) If $\mu_2 > 0$ ($\mu_2 < 0$), then Hopf bifurcation is supercritical (subcritical);*
(ii) If $\beta_2 < 0$ ($\beta_2 > 0$), then bifurcating periodic solutions are stable (unstable);
(iii) If $T_2 > 0$ ($T_2 < 0$), then the period of the bifurcating periodic solution increases (decreases).

5. Control of bifurcation using a hybrid controller

In real predator-prey systems, key parameters include the intraspecific competition coefficient among prey and the interspecific competition coefficients between predators and prey (such as growth rate, competition coefficient, predation rate). These are influenced by environmental factors (such as temperature and light). Therefore, by adjusting these parameters, the dynamics of the system can be regulated. Inspired by the methods in [28, 30], we introduce the following hybrid controller into model (1.3)

$$k_1\left(\frac{rx}{1+Ky} - \alpha x x(t-\tau) - \frac{\beta(1-m)xy}{\alpha_1 + (1-m)x + y} - E_1 x\right) + k_2[x(t-\tau) - x(t)],$$

where k_1 and k_2 represent feedback gain coefficients. $k_1 > 0$ enables the adjustment of parameters, including intraspecies interaction coefficients, interspecies interaction coefficients, and birth and death rates. In the process of adjustment, factors that influence these parameters, such as temperature that affects the birth rate, can be taken into account. The birth rate can be regulated by controlling the temperature. k_2 represents the change in the number of prey at time t. $k_2 > 0$ indicates the increase in their numbers, such as reducing harvesting, while $k_2 < 0$ indicates the decrease in their numbers through harvesting. Therefore, it is reasonable to regulate the system by adjusting the parameters and the change in prey at time t.

The following controlled prey-predator model is given by using the above hybrid controller

$$\begin{cases} \dfrac{\mathrm{d}x}{\mathrm{d}t} = k_1 \left(\dfrac{rx}{1+Ky} - \alpha x x(t-\tau) - \dfrac{\beta(1-m)xy}{\alpha_1 + (1-m)x + y} - E_1 x \right) + k_2[x(t-\tau) - x(t)], \\ \dfrac{\mathrm{d}y}{\mathrm{d}t} = \dfrac{\beta_1(1-m)xy}{\alpha_1 + (1-m)x + y} - \theta_1 y - \dfrac{E_2 y}{p_1 E_2 + p_2 y}. \end{cases} \tag{5.1}$$

The control model (5.1) has the same positive equilibrium $C^*(x^*, y^*)$ as model (1.3). Let $\tilde{x} = x - x^*$ and $\tilde{y} = y - y^*$, and drop the tilde for convenience of notation. Then, the linearized system of model (5.1) around $C^*(x^*, y^*)$ takes the following form:

$$\begin{cases} \dfrac{\mathrm{d}x}{\mathrm{d}t} = (k_1 a_{11} - k_2)x + k_1 a_{12} y + (k_1 b_{11} + k_2)x(t-\tau), \\ \dfrac{\mathrm{d}y}{\mathrm{d}t} = a_{21} x + a_{22} y, \end{cases} \tag{5.2}$$

where a_{11}, a_{12}, b_{11}, a_{21}, and a_{22} are given in (4.1). The characteristic equation of model (5.2) around $C^*(x^*, y^*)$ takes the following form:

$$\lambda^2 - (k_1 a_{11} + a_{22} - k_2)\lambda - (k_1 b_{11} + k_2)(\lambda - a_{22})e^{-\lambda\tau} + k_1 a_{11} a_{22} - k_2 a_{22} - k_1 a_{12} a_{21} = 0. \tag{5.3}$$

Assuming that

$$(H_{10}) : k_1(a_{11} + b_{11}) + a_{22} < 0,\ k_1((a_{11} + b_{11})a_{22} - a_{12}a_{21}) > 0.$$

It is easy to know that model (5.1) without delay is locally asymptotically stable at the positive equilibrium $C^*(x^*, y^*)$ if the condition (H_{10}) holds. Suppose that Eq (5.3) has a root $i\bar{\omega}$ ($\bar{\omega} > 0$), then we have

$$\begin{cases} -(k_1 b_{11} + k_2)\bar{\omega}\sin(\bar{\omega}\tau) + a_{22}(k_1 b_{11} + k_2)\cos(\bar{\omega}\tau) = \bar{\omega}^2 + (k_1(a_{12}a_{21} - a_{11}a_{22})) + k_2 a_{22}, \\ -(k_1 b_{11} + k_2)\bar{\omega}\cos(\bar{\omega}\tau) - a_{22}(k_1 b_{11} + k_2)\sin(\bar{\omega}\tau) = (k_1 a_{11} + a_{22} - k_2)\bar{\omega}. \end{cases} \tag{5.4}$$

Additionally, Eq (5.4) demonstrates that

$$G_2(\bar{Z}) := \bar{Z}^2 + \mathcal{A}_1(k_1, k_2)\bar{Z} + \mathcal{A}_2(k_1, k_2) = 0, \tag{5.5}$$

where $\bar{Z} = \bar{\omega}^2$, $\mathcal{A}_1(k_1, k_2) = k_1^2 a_{11}^2 + a_{22}^2 + 2k_1 a_{12} a_{21} - (k_1 b_{11} + k_2)^2 - 2k_1 k_2 a_{11} + k_2^2$, $\mathcal{A}_2(k_1, k_2) = k_1^2(a_{12}a_{21} - a_{11}a_{22})^2 - a_{22}^2(k_1 b_{11} + k_2)^2$. We give three conditions as follows:

$$(H_{11}) : \mathcal{A}_1(k_1, k_2) > 0 \text{ and } \mathcal{A}_2(k_1, k_2) > 0,\ (H_{12}) : \mathcal{A}_2(k_1, k_2) < 0,$$
$$(H_{13}) : (\mathcal{A}_1(k_1, k_2))^2 > 4\mathcal{A}_2(k_1, k_2) > 0,\ \mathcal{A}_1(k_1, k_2) < 0 \text{ and } \mathcal{A}_2(k_1, k_2) > 0.$$

If condition (H_{11}) is true, then Eq (5.5) has no positive root, which means that such $\bar{\omega}$ does not exist. Thus, $C^*(x^*, y^*)$ is locally asymptotically stable for all $\tau > 0$ if conditions (H_{10}) and (H_{11}) hold. Moreover, if (H_{10}) fails and (H_{11}) holds, then $C^*(x^*, y^*)$ is unstable for all $\tau > 0$.

If condition (H_{12}) is true, then Eq (5.5) admits a unique positive root $\bar{\omega}_0^2$. Substituting $\bar{\omega}_0$ into (5.4), it follows that

$$\bar{\tau}_n = \frac{1}{\bar{\omega}_0}\left[\arccos \bar{S}_1 + 2n\pi\right],$$

where $n = 0, 1, 2\cdots$, and $\bar{S}_1 = \frac{-(k_1a_{11}-k_2)\bar{\omega}_0^2-(k_1a_{11}-k_2)a_{22}^2+k_1a_{22}a_{12}a_{21}}{b_{11}(a_{22}^2+\bar{\omega}_0^2)}$.

If condition (H_{13}) is true, then Eq (5.5) has positive roots $\bar{\omega}_+^2$ and $\bar{\omega}_-^2$. Substituting $\bar{\omega}_\pm$ into (5.4), it follows that

$$\bar{\tau}_n^{\pm} = \frac{1}{\bar{\omega}_\pm}\left[\arccos \bar{S}_2 + 2n\pi\right],$$

where $n = 0, 1, 2\cdots$, and $\bar{S}_2 = \frac{-(k_1a_{11}-k_2)\bar{\omega}_\pm^2-(k_1a_{11}-k_2)a_{22}^2+k_1a_{22}a_{12}a_{21}}{b_{11}(a_{22}^2+\bar{\omega}_\pm^2)}$.

Let $\lambda(\bar{\tau}_n) = i\bar{\omega}_0$ be a root of Eq (5.3). Differentiating both sides of Eq (5.3) with respect to τ, we get

$$\left(\frac{\mathrm{d}\lambda}{\mathrm{d}\tau}\right)^{-1} = \frac{2\lambda - (k_1a_{11} + a_{22} - k_2) - (k_1b_{11} + k_2)e^{-\lambda\tau}}{-(k_1b_{11} + k_2)\lambda(\lambda - a_{22})e^{-\lambda\tau}} - \frac{\tau}{\lambda}.$$

By a series of computations, we further get

$$\mathrm{Re}\left(\frac{\mathrm{d}\lambda}{\mathrm{d}\tau}\right)^{-1}\Big|_{\tau=\bar{\tau}_n,\lambda=i\bar{\omega}_0} = \frac{G_2'(\bar{\omega}_0^2)}{(k_1b_{11} + k_2)^2(a_{22}^2 + \bar{\omega}_0^2)}.$$

When (H_{12}) holds, since $G_2(0) = \mathcal{A}_2(k_1, k_2) < 0$, $G_2(\infty) = \infty$, we obtain $G_2'(\bar{\omega}_0^2) > 0$. It is well known that

$$\mathrm{sign}\left\{\mathrm{Re}(\frac{\mathrm{d}\lambda}{\mathrm{d}\tau})\right\}_{\tau=\bar{\tau}_n,\lambda=i\bar{\omega}_0} = \mathrm{sign}\left\{\mathrm{Re}(\frac{\mathrm{d}\lambda}{\mathrm{d}\tau})^{-1}\right\}_{\tau=\bar{\tau}_n,\lambda=i\bar{\omega}_0} > 0.$$

In a similar way, let $\lambda(\bar{\tau}_n^{\pm}) = i\bar{\omega}_\pm$ be a root of Eq (5.3). When (H_{13}) holds, since $G_2(0) = \mathcal{A}_2(k_1, k_2) > 0$, $G_2(\infty) = \infty$, we obtain $G_2'(\bar{\omega}_-^2) < 0$ and $G_2'(\bar{\omega}_+^2) > 0$. Therefore, we further obtain that

$$\mathrm{sign}\left\{\mathrm{Re}(\frac{\mathrm{d}\lambda}{\mathrm{d}\tau})\right\}_{\tau=\bar{\tau}_n^-,\lambda=i\bar{\omega}_-} < 0, \quad \mathrm{sign}\left\{\mathrm{Re}(\frac{\mathrm{d}\lambda}{\mathrm{d}\tau})\right\}_{\tau=\bar{\tau}_n^+,\lambda=i\bar{\omega}_+} > 0.$$

As a consequence of the above analysis, we have the following results:

Theorem 5.1. *(i) If (H_{10}) and (H_{11}) hold, then the positive equilibrium $C^*(x^*, y^*)$ of model (5.1) is locally asymptotically stable when $\tau > 0$. If (H_{10}) fails but (H_{11}) holds, then $C^*(x^*, y^*)$ of model (5.1) is unstable when $\tau > 0$.*
(ii) If (H_{10}) and (H_{12}) hold, then $C^*(x^*, y^*)$ of model (5.1) is locally asymptotically stable when $\tau \in [0, \bar{\tau}_0)$, but unstable when $\tau > \bar{\tau}_0$. Moreover, when τ crosses the threshold value $\bar{\tau}_0$, model (5.1) loses its stability and Hopf bifurcation occurs at $C^*(x^*, y^*)$.
(iii) If (H_{10}) and (H_{13}) hold, then $C^*(x^*, y^*)$ is locally asymptotically stable for $\tau \in (0, \bar{\tau}_0^+) \cup (\bar{\tau}_0^-, \bar{\tau}_1^+) \cup \cdots \cup (\bar{\tau}_{n-1}^-, \bar{\tau}_n^+) \cup \cdots$ and unstable for $\tau \in (\bar{\tau}_0^+, \bar{\tau}_0^-) \cup (\bar{\tau}_1^+, \bar{\tau}_1^-) \cup \cdots \cup (\bar{\tau}_n^+, \bar{\tau}_n^-) \cup \cdots$. In addition, the model (5.1) undergoes a Hopf bifurcation at the positive equilibrium $C^*(x^*, y^*)$ when $\tau = \bar{\tau}_n^{\pm}$, $n = 0, 1, 2, \cdots$.

6. Numerical simulation

In this section, we are interested to carry out numerical simulations by using MATLAB software with the parameters mentioned in [8]: $r = 3$, $K = 22$, $\alpha = 0.2$, $\alpha_1 = 0.01$, $\beta = 1.5$, $\beta_1 = 0.9$, $s = 0.1$, $m = 0.8$, $E_1 = 0.9$, $E_2 = 0.001$, $p_1 = 0.9$, and $p_2 = 0.85$.

6.1. *Uncontrolled model*

The conditions (H_1)–(H_5) are verified under the above parameters. According to Theorem 3.1, there exists a unique positive equilibrium $C^*(0.4507, 0.6976)$ of model (1.3), which can be seen in Figure 1.

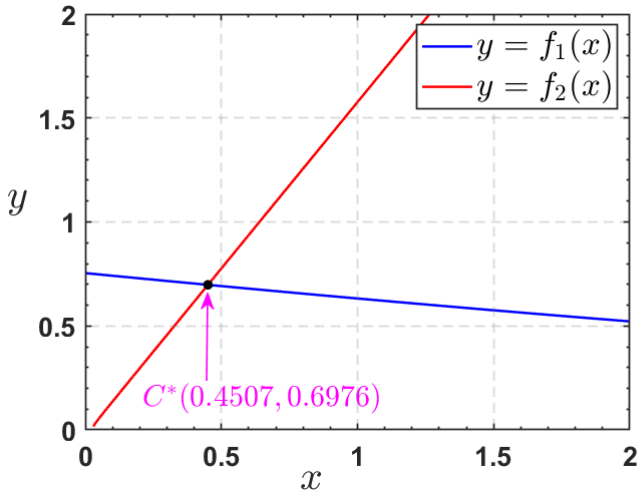

Figure 1. A unique positive equilibrium $C^*(0.4507, 0.6976)$ of model (1.3).

We can easily derive that the conditions (H_6)–(H_9) of Theorem 4.1 hold. We choose τ as a bifurcation parameter to observe Hopf bifurcation, as shown in Figure 2. From Figure 2, the positive equilibrium $C^*(0.4507, 0.6976)$ of model (1.3) is locally asymptotically stable when $0 < \tau < 6.124$, but $C^*(0.4507, 0.6976)$ is unstable when $\tau > 6.124$. Model (1.3) goes through Hopf bifurcation at the critical value $\tau_0 = 6.124$. In order to describe the rationality of the analysis results, we have drawn phase diagrams of model (1.3) with the parameters $\tau = 6$ and $\tau = 7$ (see Figure 3). Again, the properties of bifurcating periodic solutions at τ_0 are given as $C_1(0) = -15.9949 + 1.58035i$, $\mu_2 = 476.2859$, $\beta_2 = -31.9898$, and $T_2 = 1.0096$. Therefore, Hopf bifurcation is supercritical, bifurcating periodic solutions are stable, and the period of the periodic solution increases.

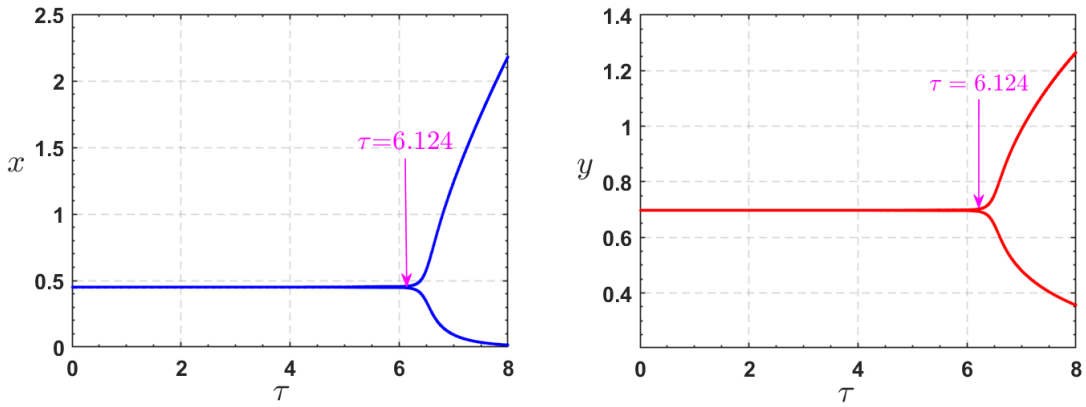

(a) (b)

Figure 2. Bifurcation diagrams of model (1.3) with respect to delay τ. (a) x, (b) y.

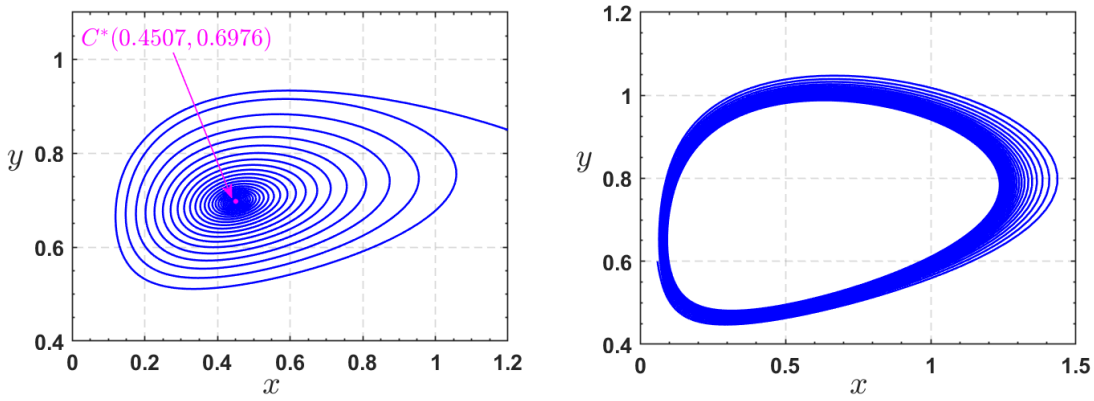

Figure 3. The dynamics of model (1.3) around $C^*(0.4507, 0.6976)$. (a) $\tau = 6 < 6.124$, (b) $\tau = 7 > 6.124$.

6.2. *Controlled model*

Based on the above numerical simulations, model (1.3) exhibits destabilizing behavior when $\tau > 6.124$. For the control model (5.1), to validate the effectiveness of the control strategy, we fixed that $\tau = 7$.

By fixing parameter $k_1 = 1$, model (5.1) is transformed into a linear time-delayed state feedback control system. Parameter k_2 is selected as the bifurcation control variable. Stability analysis is conducted at the original unstable point ($\tau = 7$) of model (1.3) to determine the stabilizing intervals with τ of model (5.1). The system remains stable for $k_2 \in I_1 = (0.0048, 0.01]$, which is seen in Figure 4.

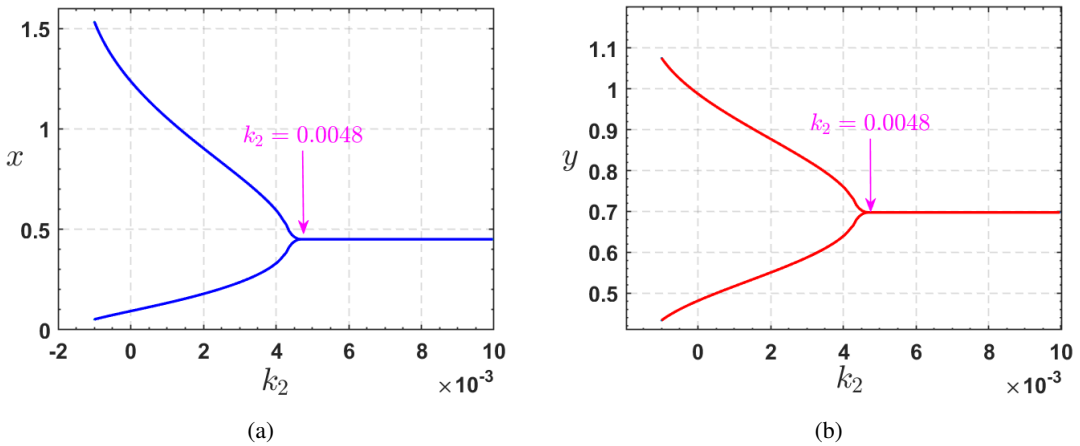

Figure 4. Bifurcation diagrams of model (5.1) with respect to parameter k_2 when $k_1 = 1$. (a) x, (b) y.

To intuitively elucidate the parameter regulation mechanism, waveform plots and phase diagrams are used to quantify the structure of stable state under varying k_2 (see Figure 5). As illustrated in Figure 5, the amplitude of oscillation is significantly suppressed as k_2 increases.

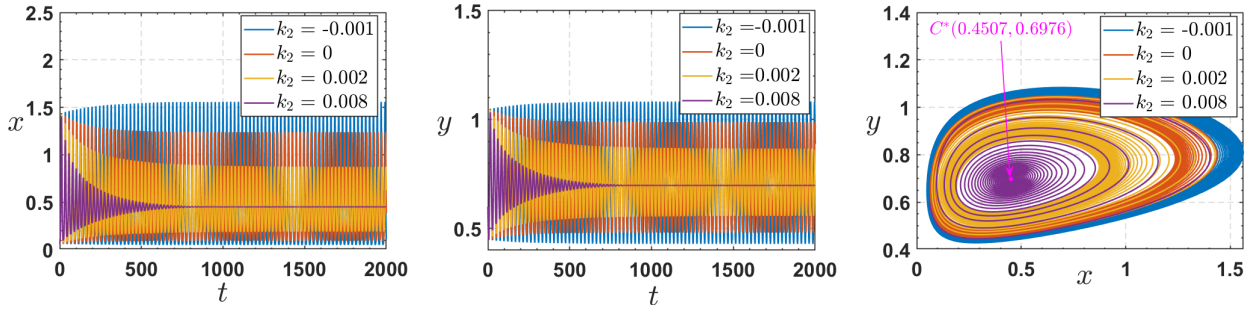

(a) (b) (c)

Figure 5. Waveform plots and phase diagram of model (5.1) with respect to different parameter k_2 when $k_1 = 1$. (a) Waveform plot of x, (b) waveform plot of y, (c) phase diagram.

Next, $k_2 = 0.01$ is selected from the stability region $I_1 = (0.0048, 0.01]$, and τ is taken as a bifurcation parameter, as shown in Figure 6. Comparing it with the uncontrolled model (1.3), it is clear that the critical value τ_0 of Hopf bifurcation is shifted from 6.124 to 7.225. When $\tau = 7$, model (5.1) is locally stable at the positive equilibrium $C^*(0.4507, 0.6976)$ when $k_2 = 0.01$ (see Figure 7(a)). Furthermore, as illustrated in Figure 7(b), when $\tau = 8$, the oscillation amplitude of Hopf bifurcation decreases with the increase of k_2. Therefore, the control parameter $k_2 = 0.01$ not only delays the critical value of Hopf bifurcation, but also suppresses the oscillation amplitude.

In fact, by fixing parameter $k_2 = 0$, model (5.1) transforms into a parameter-regulated control system. The parameter k_1 is selected as the bifurcation control variable. In the same way, when $\tau = 7$ (original unstable point), the system remains stable for $k_1 \in I_2 = (0, 0.937)$, as seen in Figure 8. To intuitively elucidate the parameter regulation mechanism, wave plots and phase diagrams are used to quantify the structure of stable state under varying k_1 (see Figure 9). As illustrated in Figure 9, the amplitude of oscillation is significantly suppressed as k_1 decreases.

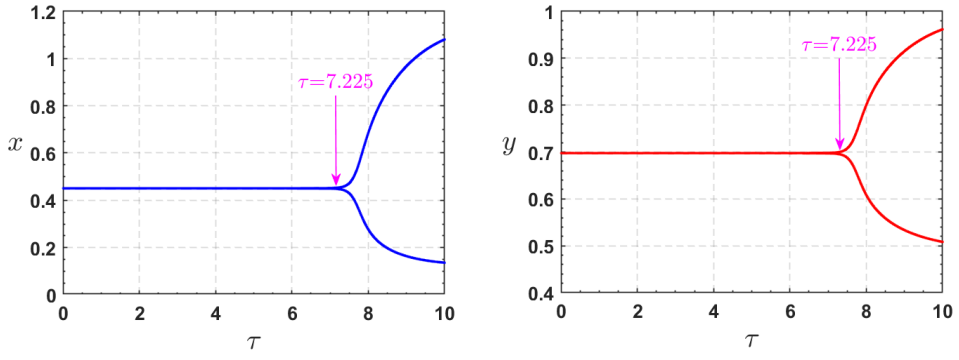

(a) (b)

Figure 6. Bifurcation diagrams of model (5.1) with respect to parameter τ when $k_1 = 1$ and $k_2 = 0.01$. (a) x, (b) y.

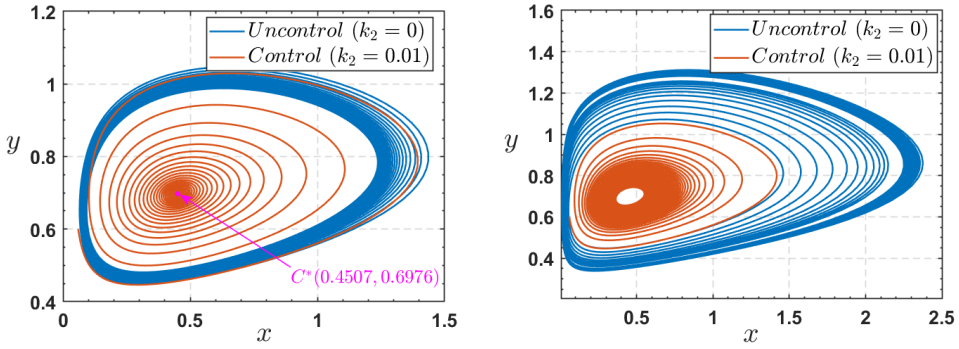

(a) (b)

Figure 7. The effect of linear time-delayed state feedback controller on Hopf bifurcation. (a) Stability changes at $\tau = 7$, (b) amplitude changes at $\tau = 8$.

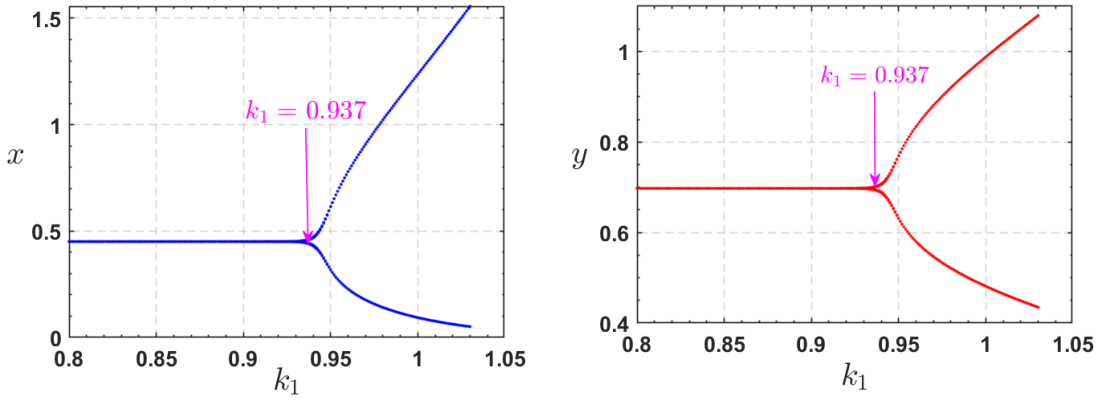

(a) (b)

Figure 8. Bifurcation diagrams of model (5.1) with respect to k_1 when $k_2 = 0$. (a) x, (b) y.

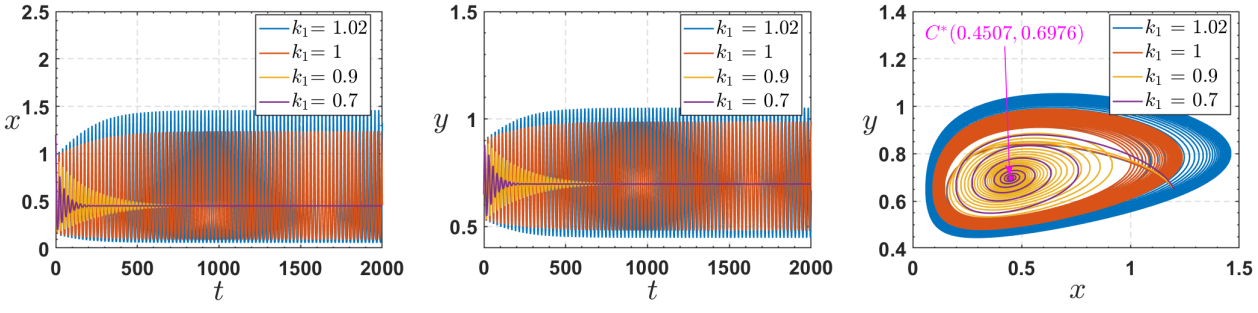

(a) (b) (c)

Figure 9. Waveform plots and phase diagram of model (5.1) with respect to different parameters k_1 when $k_2 = 0$. (a) Waveform plot of x, (b) waveform plot of y, (c) phase diagram.

Next, $k_1 = 0.8$ is selected from the stability region $I_2 = (0, 0.937)$, and τ is taken as a bifurcation parameter, as shown in Figure 10. Comparing it with the uncontrolled model (1.3), it is clear that the critical value τ_0 of Hopf bifurcation is shifted from 6.124 to 8.083. When $\tau = 7$, model (5.1) is locally stable at the positive equilibrium $C^*(0.4507, 0.6976)$ when $k_1 = 0.8$ (see Figure 11(a)). Furthermore, as illustrated in Figure 11(b), when $\tau = 10$, the oscillation amplitude of Hopf bifurcation decreases with the decrease of k_1. Therefore, the control parameter $k_2 = 0.01$ not only delays the critical value of Hopf bifurcation, but also suppresses the oscillation amplitude.

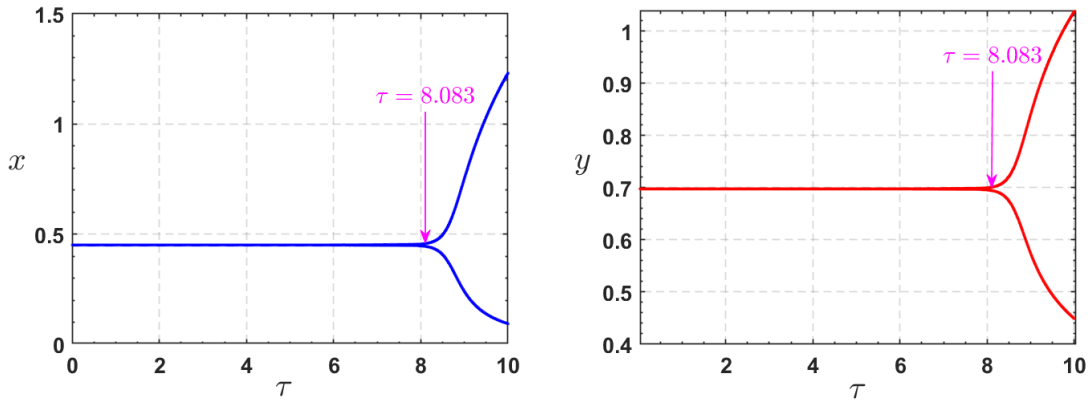

(a) (b)

Figure 10. Bifurcation diagrams of model (5.1) with respect to parameter τ when $k_1 = 0.8$ and $k_2 = 0$. (a) x, (b) y.

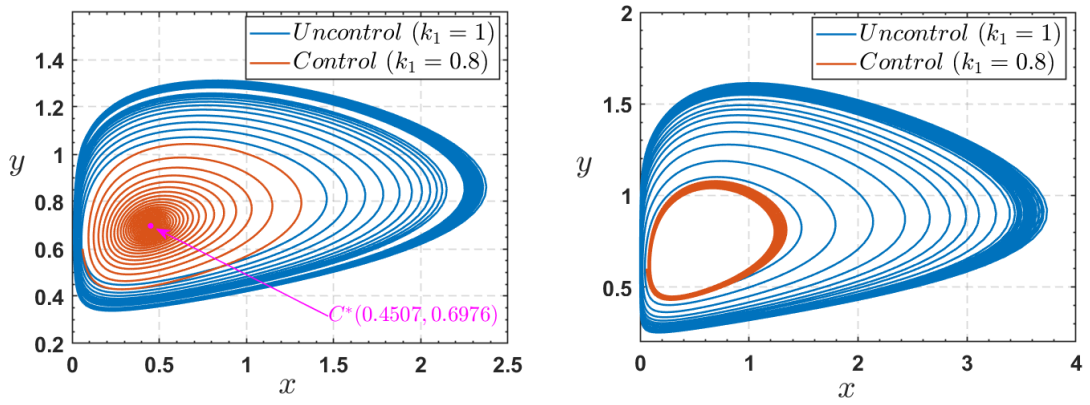

(a) (b)

Figure 11. The effect of parameter-regulated controller on Hopf bifurcation. (a) Stability changes at $\tau = 7$, (b) amplitude changes at $\tau = 10$.

From the ecological point of view, numerical simulations demonstrate that in the absence of a controller, the positive equilibrium becomes unstable due to delay, triggering a Hopf bifurcation. However, the unstable equilibrium can be stabilized through the implementation of a linear time-delayed state feedback controller or a parameter-regulated controller. These findings confirm that

only time-delayed state feedback controllers or parameter-regulated controllers can effectively suppress the amplitude of periodic solutions, while significantly expanding its delay-dependent stability range required for the stability of the predator-prey system.

However, as τ increases, neither a linear time-delayed state feedback controller nor a parameter-regulated controller alone can eliminate Hopf bifurcation and restore its stability. For instance, when $\tau = 10$, we compare waveform plots and phase diagrams under four parameter sets: $(k_1, k_2) = (1, 0), (1, 0.01), (0.8, 0)$, and $(0.8, 0.01)$ (see Figure 12). Here, $(1, 0)$ corresponds to the case without control, $(1, 0.01)$ represents the case of time-delayed state feedback control, $(0.8, 0)$ denotes the case of parameter regulation, and $(0.8, 0.01)$ signifies the case of the hybrid control scheme combining time-delayed state feedback and parameter regulation. Figure 12 demonstrates that only the hybrid controller can eliminate Hopf bifurcation when $\tau = 10$, thereby stabilizing the system.

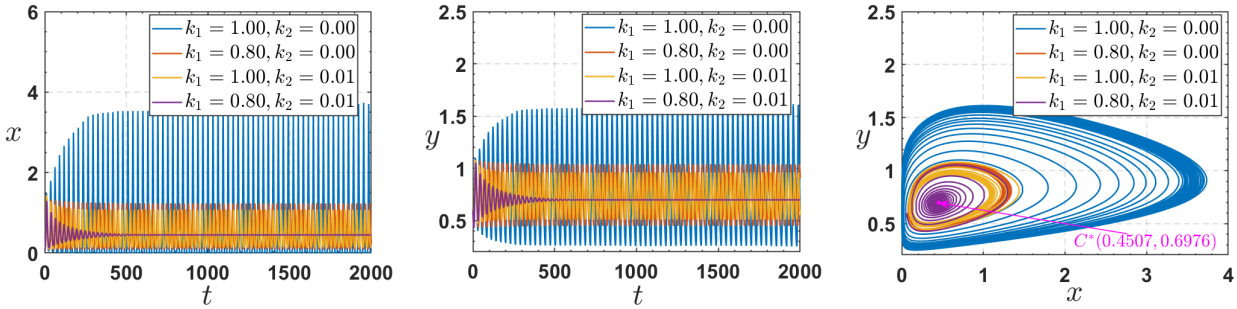

(a) (b) (c)

Figure 12. Waveform plots and phase diagram of model (5.1) with respect to different parameters k_1 and k_2 when $\tau = 10$. (a) Waveform plot of x, (b) waveform plot of y, (c) phase diagram.

To further investigate the impact of the hybrid controller on the stability range of delay τ, we select fixed parameters $k_1 = 0.85$ and $k_2 = 0.008$ and plot the bifurcation diagram of model (5.1) with respect to τ, as shown in Figure 13. The results demonstrate that as the delay τ increases, the positive equilibrium $C^*(0.4507, 0.6976)$ is locally asymptotically stable within the intervals $(0, 9.76) \cup (14.46, 34.06) \cup (44.16, 58.36) \cup (74.21, 83.01)$, but is unstable within the intervals $(9.76, 14.46) \cup (34.06, 44.16) \cup (58.36, 74.21) \cup (83.01, 100]$. Hopf bifurcations occur at critical values $\bar{\tau}_0^+ = 9.76$, $\bar{\tau}_0^- = 14.46$, $\bar{\tau}_1^+ = 34.06$, $\bar{\tau}_1^- = 44.16$, $\bar{\tau}_2^+ = 58.36$, $\bar{\tau}_2^- = 74.21$, and $\bar{\tau}_3^+ = 83.01$, corresponding to transitions in stability states.

To elucidate the multiple stability transitions induced by the hybrid controller, waveform plots are plotted by selecting representative τ values from distinct regions of the bifurcation diagram. From Figure 14, it can be seen that the system exhibits multi-time-scale oscillations: different stability switching points correspond to different oscillatory modes of model (5.1) (with different periods and amplitudes). This implies that population fluctuations may not follow a single pattern but instead exhibit different fluctuation characteristics under different conditions. This indicates that the hybrid controller not only extends the stability intervals of the system with respect to τ, but also enables τ itself to function as a stability switch. From a biological perspective, this stability-switching phenomenon reveals the complexity and fragility of the predator-prey model. This mechanism is the key intrinsic factor for understanding phenomena, such as the collapse of island populations and the

periodic outbreaks of agricultural pests, and it also serves as the theoretical foundation for ecological management through the regulation of delay targets.

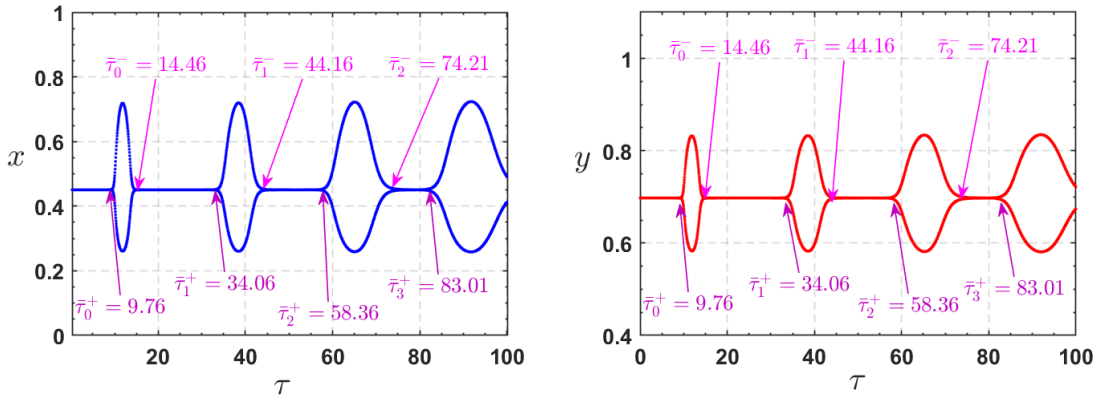

(a) (b)

Figure 13. Bifurcation diagrams of model (5.1) with respect to parameter τ when $k_1 = 0.85$ and $k_2 = 0.008$. (a) x, (b) y.

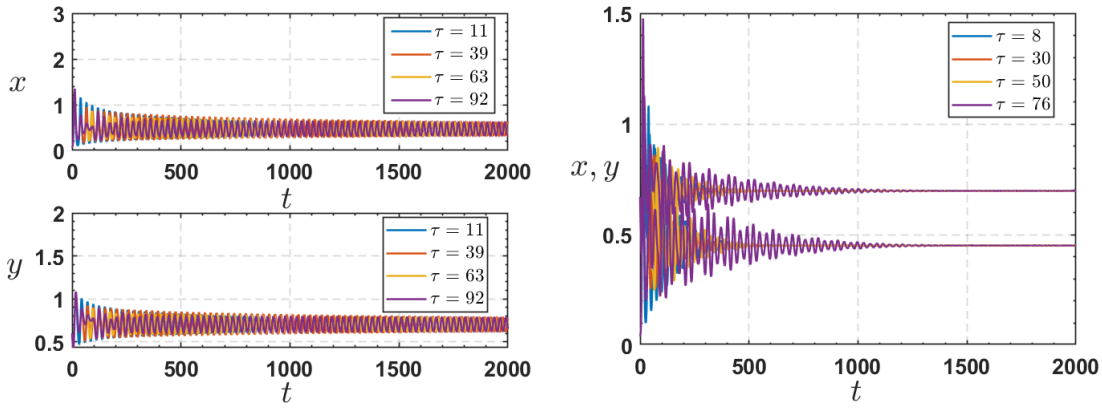

(a) (b)

Figure 14. Waveform plots of model (5.1) with respect to different parameters τ. (a) Stable, (b) unstable.

Furthermore, when $k_1 = 0.8$ and $k_2 = 0.01$, taking the delay τ as the bifurcation parameter, we predict the stability of the system at positive equilibrium $C^*(0.4507, 0.6976)$ within the desired delay range $(0, 100]$, as shown in Figure 15(a). The results indicate that the system maintains stability throughout the entire interval $\tau \in (0, 100]$. This demonstrates that the Hopf bifurcation presented in the original system has been eliminated. Through the hybrid control strategy, the originally unstable state has been transformed into an asymptotically stability state, as shown in Figure 15(b). This implies that predator and prey can converge to constant values, thereby achieving long-term stability. Thus, our numerical results effectively validate the accuracy of the theoretical model. This study holds significant ecological importance, providing quantitative theoretical support for the sustainable state

of populations in natural ecosystems.

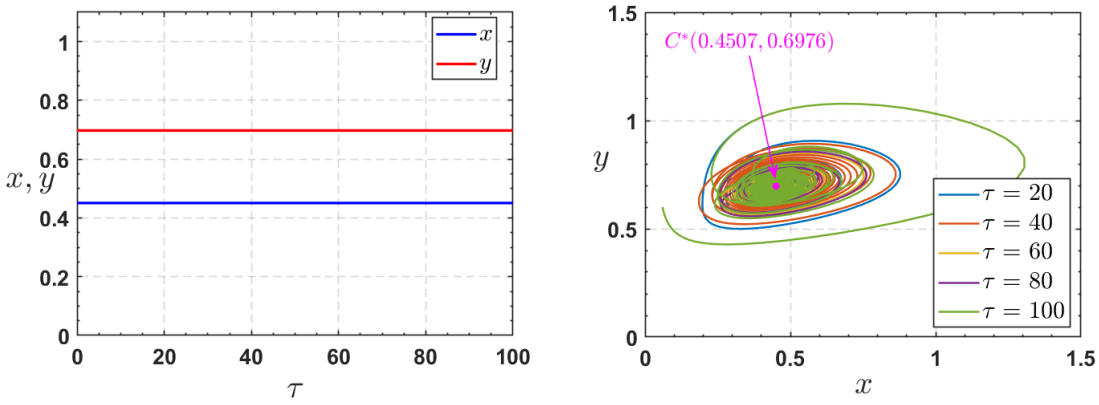

(a) (b)

Figure 15. Bifurcation diagram and phase diagram of model (5.1) with respect to parameters τ. (a) Bifurcation diagram with respect to parameter τ with $k_1 = 0.8$ and $k_2 = 0.01$, (b) phase diagram with different τ.

7. Discussion and conclusions

Wang et al. [4] investigated the impact of the fear effect of predator in a Beddington-DeAngelis type predator-prey model with prey refuge. They analyzed various bifurcations, including transcritical bifurcation, saddle-node bifurcation, Hopf bifurcation, and two-dimensional Bogdanov-Takens bifurcation. In this paper, we mainly focus on Hopf bifurcation and hybrid control strategy in a predator-prey model with delay. We analyze the conditions and critical values for Hopf bifurcation in model (1.3) and its controlled model (5.1) from both theoretical and numerical simulation perspectives.

For model (1.3), when the delay exceeds the critical value 6.124, Hopf bifurcation occurs. When the delay exceeds 8, the prey goes extinct. The predator is sustained by its internal energy reserves for a brief period but ultimately becomes extinct as well. The results demonstrate that in the delayed predator-prey model, the self-feedback delay induced by prey competition for resources can regulate system stability. When employing only a linear time-delayed state feedback controller or a parameter-regulated controller, not only is the critical value of delay for Hopf bifurcation delayed, but also the oscillation amplitude of the periodic solutions is effectively suppressed. However, when the delay is further increased, using solely a linear time-delayed state feedback controller or a parameter-regulated controller can no longer control the Hopf bifurcation. After implementing a hybrid controller, the system maintains locally asymptotical stability over a given large range of delay, significantly extending the global stability region with respect to the delay. This strategy effectively eliminates the extinction risk driven by delays and achieves a dual stabilization mechanism.

It is noteworthy that the measure of interference of an individual predator is not considered in the model constructed; then, the response function degenerates into the standard Holling II. Moreover, if prey refuge, linear harvesting of prey, and nonlinear harvesting of predator are zero, our model is transformed into the model formulated by Wang et al. [4]. In light of this characteristic, they considered the cost of fear effect into the reproduction term of prey, proposed the following predator-

prey model with Holling II, and studied whether fear effect can exert an influence on prey, and to what extent. If the impact of predator interference intensity on the functional response is neglected, and harvesting effects on both prey and predator are not considered, our model reduces to the model proposed in [5]. Zhang et al. [5] demonstrated that fear effect and refuge effect availability can induce Hopf bifurcation in the system. Given the significant influence of interference intensity on the functional response, Wang et al. [8] further investigated the model with effects of fear, refuge, harvesting, and the Beddington-DeAngelis-type functional response and analyzed various bifurcations, including transcritical bifurcation, saddle-node bifurcation, Hopf bifurcation, and two-dimensional Bogdanov-Takens bifurcation. Building upon these works, we further examine the regulatory role of self-feedback delay (induced by competition for environmental resources of prey) on system stability and address the control of Hopf bifurcation by using a hybrid controller. This study has made two advancements in the stability of delay system: establishing stability conditions for arbitrary delay when control gains are unknown, providing a basis for gains selection, and determining the maximum stable delay interval when gains are known, supporting the introduction of delay by humans to optimize performance. Consequently, the results are also applicable to the models presented in [4, 5].

In future research, to enhance the model's practicality, it would be necessary to consider the delayed growth of prey resulting from the fear effect induced by predators. This factor can be incorporated into our prey-predator system, namely

$$\begin{cases} \dfrac{\mathrm{d}x}{\mathrm{d}t} = rx\left(\dfrac{1}{1+Ky(t-\tau_1)} - \dfrac{x(t-\tau_2)}{k}\right) - \dfrac{\beta(1-m)xy}{\alpha_1+(1-m)x+y} - q_1Ax, \\ \dfrac{\mathrm{d}y}{\mathrm{d}t} = \dfrac{\beta_1(1-m)xy}{\alpha_1+(1-m)x+y} - \theta_1 y - \dfrac{q_2By}{p_1q_2B+p_2y}, \end{cases} \tag{7.1}$$

where τ_1 is the delay period of the fear effect on plant's growth, and τ_2 is the delay of a self-feedback delay induced by prey competition for resources. Given the effectiveness of hybrid controller in expanding the stability region of the delayed predator-prey system and reducing extinction risks, a key focus for future research is addressing its implementation costs. An optimal control function can be constructed to minimize control costs while ensuring the system's local stability at the positive equilibrium (within the desired delay range). This dual-objective optimization aims to achieve both stability and economic efficiency. Efficiently solving this optimization problem and applying it to complex ecosystems represents a critical frontier requiring breakthroughs. It demands the development of innovative methods at the intersection of ecosystem modeling and control theory to address challenges posed by system complexity, delay effect, and multi-objective trade-offs. We leave this work to the future.

Author contributions

J.-G. W.: Conceptualization, Methodology, Software, Validation, Formal analysis, Investigation, Writing–original draft, Writing–reviewing and editing, Visualization; X.-Y. M.: Conceptualization, Validation, Investigation, Writing–reviewing and editing, Visualization, Supervision. All authors have read and agreed to the published version of the manuscript.

Use of Generative-AI tools declaration

The authors declare they have not used Artificial Intelligence (AI) tools in the creation of this article.

Acknowledgments

This work is supported by the National Natural Science Foundation of China (Grant No. 12161054 and 12161011), Funds for Innovative Fundamental Research Group Project of Gansu Province (Grant No. 24JRRA778), and the Doctoral Foundation of Lanzhou University of Technology.

Conflict of interest

The authors declare that they have no known competing financial interests or personal relationships that could have appeared to influence the work reported in this paper.

References

1. A. J. Lotka, Analytical note on certain rhythmic relations in organic systems, *Proc. Natl. Acad. Sci. U.S.A.*, **6** (1920), 410–415. https://doi.org/10.1073/pnas.6.7.410
2. V. Volterra, Fluctuations in the abundance of a species considered mathematically, *Nature*, **118** (1926), 558–560. https://doi.org/10.1038/118558a0
3. S. G. Mortoja, P. Panja, S. K. Mondal, Dynamics of a predator-prey model with nonlinear incidence rate, Crowley-Martin type functional response and disease in prey population, *Ecological Genetics and Genomics*, **10** (2019), 100035. https://doi.org/10.1016/j.egg.2018.100035
4. X. Wang, L. Zanette, X. Zou, Modelling the fear effect in predator-prey interactions, *J. Math. Biol.*, **73** (2016), 1179–1204. https://doi.org/10.1007/s00285-016-0989-1
5. H. Zhang, Y. Cai, S. Fu, W. Wang, Impact of the fear effect in a prey-predator model incorporating a prey refuge, *Appl. Math. Comput.*, **356** (2019), 328–337. https://doi.org/10.1016/j.amc.2019.03.034
6. L. Y. Ning, D. Wu, T. C. Feng, S. J. Hu, G.-L. Feng, Y. P. Wu, The role of weak prey refuge in the cooperation-competition balance of prey-predator systems, *Nonlinear Dyn.*, **113** (2025), 7535–7552. https://doi.org/10.1007/s11071-024-10498-x
7. D. Hu, H. Cao, Stability and bifurcation analysis in a predator-prey system with Michaelis-Menten type predator harvesting, *Nonlinear Anal. Real*, **33** (2017), 58–82. https://doi.org/10.1016/j.nonrwa.2016.05.010
8. J. G. Wang, X. Y. Meng, L. Lv, J. Li, Stability and bifurcation analysis of a Beddington-DeAngelis prey-predator model with fear effect, prey refuge and harvesting, *Int. J. Bifurcat. Chaos*, **33** (2023), 2350013. https://doi.org/10.1142/S021812742350013X
9. W. Li, W. Zhao, J. Cao, L. Huang, Dynamics of a linear source epidemic system with diffusion and media impact, *Z. Angew. Math. Phys.*, **75** (2024), 144. https://doi.org/10.1007/s00033-024-02271-2

10. S. X. Wu, X. Y. Meng, Hopf bifurcation analysis of a multiple delays stage-structure predator-prey model with refuge and cooperation, *Electron. Res. Arch.*, **33** (2025), 995–1036. https://doi.org/10.3934/era.2025045

11. N. H. Gazi, M. Bandyopadhyay, Effect of time delay on a harvested predator-prey model, *J. Appl. Math. Comput.*, **26** (2008), 263–280. https://doi.org/10.1007/s12190-007-0015-2

12. Y. Wang, X.-Y. Meng, Bifurcation and control of a delayed Leslie-Gower fractional-order predator-prey model with fear effect and prey refuge, *Adv. Cont. Discr. Mod.*, **2025** (2025), 103. https://doi.org/10.1186/s13662-025-03959-z

13. W. J. Li, L. A. Yang, J. D. Cao, Threshold dynamics of a degenerated diffusive incubation period host–pathogen model with saturation incidence rate, *Appl. Math. Lett.*, **160** (2025), 109312. https://doi.org/10.1016/j.aml.2024.109312

14. X.-Y. Meng, Z.-W. Liang, Dynamics analysis of a delayed diffusive predator-prey model with memory-based diffusion and fear effect of prey, *Int. J. Biomath.*, In press. https://doi.org/10.1142/S1793524525501013

15. X. Han, F. Xia, P. Ji, Q. Bi, J. Kurths, Hopf-bifurcation-delay-induced bursting patterns in a modified circuit system, *Commun. Nonlinear Sci.*, **36** (2016), 517–527. https://doi.org/10.1016/j.cnsns.2016.01.001

16. Q. Xue, G. Q. Sun, C. Liu, Z.-G. Guo, Z. Jin, Y.-P. Wu, et al., Spatiotemporal dynamics of a vegetation model with nonlocal delay in semi-arid environment, *Nonlinear Dyn.*, **99** (2020), 3407–3420. https://doi.org/10.1007/s11071-020-05486-w

17. Z. Zhu, R. Wu, F. Chen, Z. Li, Dynamic behaviors of a Lotka-Volterra commensal symbiosis model with non-selective Michaelis-Menten type harvesting, *IAENG Int. J. Appl. Math.*, **50** (2020), 396–404.

18. D. M. Anderson, Turning back the harmful red tide, *Nature*, **388** (1997), 513–514. https://doi.org/10.1038/41415

19. S. Pandey, U. Ghosh, D. Das, S. Chakraborty, A. Sarkar, Rich dynamics of a delay-induced stage-structure prey-predator model with cooperative behaviour in both species and the impact of prey refuge, *Math. Comput. Simul.*, **216** (2024), 49–76. https://doi.org/10.1016/j.matcom.2023.09.002

20. G. Chen, D. J. Hill, X. Yu, *Bifurcation control: theory and applications*, 1 Eds., Heidelberg: Springer, 2003. https://doi.org/10.1007/b79665

21. R. M. May, Biological populations with nonoverlapping generations: stable points, stable cycles, and chaos, *Science*, **186** (1974), 645–647. https://doi.org/10.1126/science.186.4164.645

22. A. Q. Khan, M. L. Alsulami, Complicate dynamical analysis of a discrete predator-prey model with a prey refuge, *AIMS Math.*, **8** (2023), 15035–15057. https://doi.org/10.3934/math.2023768

23. L. Zhang, Q. Han, Z. Fang, S. Peng, Anti-control of Hopf bifurcation for the Willamowski-Rössler system, *Int. J. Dyn. Control*, **12** (2024), 1562–1570. https://doi.org/10.1007/s40435-023-01264-9

24. M. S. Shabbir, Q. Din, M. De la Sen, J. F. Gómez-Aguilar, Exploring dynamics of plant-herbivore interactions: bifurcation analysis and chaos control with Holling type-II functional response, *J. Math. Biol.*, **88** (2024), 8. https://doi.org/10.1007/s00285-023-02020-5

25. S. Biswas, P. K. Tiwari, S. Pal, Delay-induced chaos and its possible control in a seasonally forced eco-epidemiological model with fear effect and predator switching, *Nonlinear Dyn.*, **104** (2021), 2901–2930. https://doi.org/10.1007/s11071-021-06396-1

26. T. Vijayalakshmi, R. Senthamarai, Application of homotopy perturbation and variational iteration methods for nonlinear imprecise prey-predator model with stability analysis, *J. Supercomput.*, **78** (2022), 2477–2502. https://doi.org/10.1007/s11227-021-03956-5

27. D. Li, H. Liu, H. Zhang, M. Ma, Y. Ye, Y. Wei, Bifurcation analysis in a predator-prey model with an Allee effect and a delayed mechanism, *Acta Math. Sci.*, **43** (2023), 1415–1438. https://doi.org/10.1007/s10473-023-0324-z

28. Y. Lu, M. Xiao, J. Liang, J. Ding, Y. Zhou, Y. Wan, et al., Hybrid control synthesis for Turing instability and Hopf bifurcation of marine planktonic ecosystems with diffusion, *IEEE Access*, **9** (2021), 111326–111335. https://doi.org/10.1109/ACCESS.2021.3103446

29. Q. Cui, C. Xu, W. Ou, Y. Pang, Z. Liu, P. Li, et al., Bifurcation behavior and hybrid controller design of a 2D Lotka-Volterra commensal symbiosis system accompanying delay, *Mathematics*, **11** (2023), 4808. https://doi.org/10.3390/math11234808

30. Y. Mu, W. C. Lo, Y. Tan, Z. Liu, Hybrid control for the prey in a spatial prey-predator model with cooperative hunting and fear effect time lag, *Appl. Math. Comput.*, **491** (2025), 129217. https://doi.org/10.1016/j.amc.2024.129217

31. L. Pei, S. Wang, Double Hopf bifurcation of differential equation with linearly state-dependent delays via MMS, *J. Appl. Math. Comput.*, **341** (2019), 256–276. https://doi.org/10.1016/j.amc.2018.08.040

32. P. Li, R. Gao, C. Xu, J. Shen, S. Ahmad, Y. Li, Exploring the impact of delay on Hopf bifurcation of a type of BAM neural network models concerning three nonidentical delays, *Neural Process. Lett.,* **55** (2023), 11595–11635. https://doi.org/10.1007/s11063-023-11392-0

33. W. Ou, C. Xu, Q. Cui, Y. Pang, Z. Liu, J. Shen, et al., Hopf bifurcation exploration and control technique in a predator-prey system incorporating delay, *AIMS Math.*, **9** (2024), 1622–1651. https://doi.org/10.3934/math.2024080

34. S. Wiggins, *Introduction to applied nonlinear dynamical systems and chaos*, 2 Eds., New York: Springer, 2003. https://doi.org/10.1007/b97481

35. A. Granas, J. Dugundji, *Fixed point theory*, 1 Eds., New York: Springer, 2003. https://doi.org/10.1007/978-0-387-21593-8

36. J. E. Marsden, M. McCracken, *The Hopf bifurcation and its applications*, 1 Eds., New York: Springer, 1976. https://doi.org/10.1007/978-1-4612-6374-6

37. Y. Kuang, *Delay differential equations with applications in population dynamics*, Boston: Academic Press, 1993.

AIMS Press

© 2025 the Author(s), licensee AIMS Press. This is an open access article distributed under the terms of the Creative Commons Attribution License (https://creativecommons.org/licenses/by/4.0)